Published in final edited form as:
Toxicol Pathol. 2013 February ; 41(2): 151–180. doi:10.1177/0192623312467102.

Proceedings of the 2012 National Toxicology Program Satellite Symposium

SUSAN A. ELMORE[1], **BRIAN R. BERRIDGE**[2], **MICHAEL C. BOYLE**[1], **MICHELLE C. CORA**[1], **MARK J. HOENERHOFF**[1], **LINDA KOOISTRA**[3], **VICTORIA A. LAAST**[4], **JAMES P. MORRISON**[3], **DEEPA RAO**[5], **MATTHIAS RINKE**[6], and **KATSUHIKO YOSHIZAWA**[7]

[1]National Toxicology Program, National Institute of Environmental Health Sciences, National Institutes of Health, Research Triangle Park, North Carolina, USA

[2]GlaxoSmithKline, Raleigh, North Carolina, USA

[3]Charles River Laboratories, Pathology Associates, Durham, North Carolina, USA

[4]Covance Pharmaceutical R&D Co. Ltd., Shanghai, China

[5]Integrated Laboratory Systems, Inc., Research Triangle Park, North Carolina, USA

[6]Bayer Pharma AG, Wuppertal, Germany

[7]Kansai Medical University, Osaka, Japan

Abstract

The 2012 annual National Toxicology Program (NTP) Satellite Symposium, entitled “Pathology Potpourri,” was held in Boston in advance of the Society of Toxicologic Pathology’s 31st annual meeting. The goal of the NTP Symposium is to present current diagnostic pathology or nomenclature issues to the toxicologic pathology community. This article presents summaries of the speakers’ presentations, including diagnostic or nomenclature issues that were presented, along with select images that were used for audience voting or discussion. Some lesions and topics covered during the symposium include eosinophilic crystalline pneumonia in a transgenic mouse model; differentiating adrenal cortical cystic degeneration from adenoma; atypical eosinophilic foci of altered hepatocytes; differentiating cardiac schwannoma from cardiomyopathy; diagnosis of cardiac papillary muscle lesions; intrahepatocytic erythrocytes and venous subendothelial hepatocytes; lesions in Rathke’s cleft and pars distalis; pernicious anemia and megaloblastic disorders; embryonic neuroepithelial dysplasia, holoprosencephaly and exencephaly; and INHAND nomenclature for select cardiovascular lesions.

Address correspondence to: Susan A. Elmore, National Toxicology Program, Cellular and Molecular Pathology Branch, National Institute of Environmental Health Sciences, National Institutes of Health, Research Triangle Park, NC 27709, USA; elmore@niehs.nih.gov..

The author(s) declared no potential conflicts of interest with respect to the research, authorship, and/or publication of this article.

Keywords

NTP Satellite Symposium; eosinophilic crystalline pneumonia; adrenal cortex adenoma; cortical cystic degeneration; atypical foci of altered hepatocytes; cardiac schwannoma; cardiomyopathy; myocardial necrosis; myocardial fibrosis; pancreatic ductal cell adenoma; intrahepatocytic erythrocytes; subendothelial hepatocytes; Rathke's cleft; pernicious anemia; megaloblastic anemia; neuroepithelial dysplasia; holoprosencephaly; exencephaly

Introduction

The National Toxicology Program (NTP) Satellite Symposium is a 1-day meeting that is traditionally held in conjunction with the annual Society of Toxicologic Pathology (STP) meeting (Bach et al. 2010; Adams et al. 2011). Attendance at the symposium has steadily increased since the first meeting in 2000, and this year there were 260 registered participants. The objective of this annual symposium is to provide continuing education on interpreting histopathology slides. This includes the presentation and discussion of diagnostically difficult, interesting, or rare lesions, or challenging nomenclature issues. The session is interactive in that each speaker presents images for audience voting via wireless keypads. Once the votes are tallied, the results are displayed on the screen for all to view. The speaker generally provides his or her preferred diagnosis for comparison with some additional background information, after which lively and constructive discussion ensues.

The theme for the 2012 Symposium was "Pathology Potpourri," which allowed for a variety of topics to be presented. Species included rat and mouse, and organ systems included lung, adrenal gland, liver, heart, pancreas, and pituitary. Three cases of embryonic lesions were also presented. A clinical pathology case of pernicious anemia and megaloblastic disorders with challenging erythron data and blood smears was included. One speaker presented diagnostic challenges that the International Harmonization of Nomenclature and Diagnostic Criteria (INHAND) Cardiovascular Subcommittee had been considering. This article provides synopses of all presentations including the diagnostic or nomenclature issues, a selection of images presented for voting and discussion, voting choices, voting results, and major discussion points.

Eosinophilic Crystalline Pneumonia

The symposium began with a presentation given by Dr. Mark Hoenerhoff (NTP, National Institute of Environmental Health Sciences [NIEHS], Research Triangle Park, NC), featuring an interesting lung lesion in a colony of transgenic mice. The aim of this presentation was to address nomenclature surrounding the lesion and to showcase interesting collaborative projects undertaken by NTP pathologists with the Division of Intramural Research at the NIEHS.

Male and female mice in this study presented with clinical signs of poor weight gain, ruffled hair coat, hunched posture, and rapid breathing. At necropsy evaluation, the lungs failed to collapse upon opening the thorax and were diffusely firm and mottled whitish tan to red. Histologically, the lungs were diffusely affected by a marked inflammatory infiltrate

composed of large epithelioid macrophages and occasional multinucleate giant cells expanding alveolar spaces and airways (Figure 1A). Small numbers of mature and degenerate neutrophils were scattered within alveolar spaces and often accompanied macrophages and degenerate cellular debris within bronchioles. Macrophages and multinucleate giant cells were distended with large amounts of eosinophilic amorphous to granular cytoplasm containing large numbers of fine acicular crystalline material. In some areas, few large needle-shaped crystals could be seen extracellularly. Other characteristics of this lesion were variable and consisted of multifocal alveolar wall thickening, type II pneumocyte hyperplasia, peribronchiolar fibrosis (Figure 1B), and bronchiolar epithelial hyperplasia (Figure 1C).

The eight voting choices presented to the audience were (1) granulomatous pneumonia, (2) acidophilic macrophage pneumonia, (3) histiocytic pneumonia, (4) eosinophilic crystalline pneumonia, (5) alveolar proteinosis, (6) crystalline pneumonitis, (7) histiocytic infiltrate, and (8) other. The most popular answer from the participants was eosinophilic crystalline pneumonia ([ECP] 53% of respondents), which is consistent with the current nomenclature in the scientific literature. “Acidophilic macrophage pneumonia” (31% of respondents) and “crystalline pneumonitis” (3% of respondents), while considered accurate diagnoses, are older terms that are not currently in use in the scientific literature. While diagnoses of “granulomatous” (2%) or “histiocytic” (6%) pneumonia would also have been considered, these are not the most accurate or descriptive diagnostic terms for the unique characteristics of the lesion. “Histiocytic infiltrate” (0%) is characterized by a relatively mild influx of morphologically normal histiocytes rather than the unique epithelioid macrophages and multinucleate cells in this lesion, so this diagnosis was not considered appropriate. Finally, “alveolar proteinosis” (5%) was not considered as a correct diagnosis since this lesion is characterized by the accumulation of large amounts of proteinaceous fluid within alveolar spaces due to a macrophage functional defect.

ECP is an idiopathic background lesion in wild-type mice of various strains. The severity and incidence of the lesion is significantly influenced by background strain and genotype. ECP is common in C57BL/6 and 129 strains as well as their derivatives (Guo, Johnson, and Schuh 2000; Harbord et al. 2002; Murray and Luz 1990) and has been found to be a major cause of fatality in aging 129S4/SvJae mice (Hoenerhoff, Starost, and Ward 2006; Ward et al. 2001). It is a common finding in a number of genetically engineered mouse models and strains that are prone to immunopathic disease, including those with altered immune function such as the $p47^{phox}$ and $gp91^{phox}$ knockout mouse models, which are deficient in enzymes needed to generate superoxide, hydrogen peroxide, and hydroxyl radicals necessary for intracellular killing of bacteria (France and Muir 2000; Harbord et al. 2002; Liu et al. 2009). Immunocompromised strains such as the “motheaten” mouse (a mutant C57BL/6 strain) (Shultz et al. 1984; Ward 1978) and severe combined immunodeficient (SCID) mice (Guo, Johnson, and Schuh 2000) also develop the disease. While ECP commonly occurs spontaneously in susceptible strains, it may be exacerbated by a variety of concurrent inflammatory, allergic, and neoplastic diseases (Murray and Luz 1990). ECP is commonly found in association with pulmonary adenomas (Guo, Johnson, and Schuh 2000), allergic airway disease and asthma (Webb, McKenzie, and Foster 2001; Zhao et al. 2005), and infectious and inflammatory processes (Harbord et al. 2002; Hung et al. 2002).

In general, ECP has a variable severity from mild and asymptomatic to fulminating and fatal. The character of the lesion may be quite broad, ranging from focal infiltrates to diffuse, as in this case. Often dense lymphoplasmacytic perivascular and/or peribronchiolar cuffing accompanies the lesion. Crystals within the lesion may range from small, intracytoplasmic crystalline material to large, angular to polygonal extracellular material, and multinucleate giant cells may often be quite large, containing up to dozens of nuclei in some cells. Ultrastructural evaluation of this case revealed alveolar macrophages within the lesion that were markedly distended with intracytoplasmic needle-like inclusions (Figure 1D), which at higher magnification were composed of electron-dense granular material that lacked a periodic structure, and were membrane bound (Figure 1E). Therefore, these structures are in fact not crystals but rather crystalloid arrays. Since they are membrane bound, material within these arrays may be accumulating within degenerate mitochondria, lysosomes, or endoplasmic reticulum. In fact, these arrays often appeared to be associated with degenerate mitochondria. Similar membrane-bound material has been shown to accumulate in degenerating mitochondria as a result of cellular toxicity and mitochondrial dysfunction (Nathaniel 1980; Suski et al. 2011; Svoboda and Manning 1964). However, other investigators have demonstrated Chi3l3 protein within the rough endoplasmic reticulum (Nio et al. 2004). In this case, the severity and chronicity of the lesion precludes identification of the organelles in which this material has accumulated. Regardless, it does seem to represent a general dysfunction in the metabolism of these alveolar macrophages. Interestingly, macrophages containing such crystalline arrays were not restricted to the lung in these animals. We observed similar inclusions within Kupffer cells in the liver (Figure 1F), suggesting that this lesion represents a global or systemic antigen-presenting cell defect, although in this case the inclusions were most phenotypically prevalent in the lung. Alternatively, the presence of this material in Kupffer cells may reflect extrusion of the protein from the lesion in the lung into the vasculature and phagocytosis by Kupffer cells in the liver.

Macrophages, multinucleate cells, and crystalline material within these lesions are immunoreactive for Ym1 protein, recently renamed as chitinase 3–like 3 (or Chi3l3) protein (Figure 1G). Chi3l3 is a member of the chitinase-like family of proteins; however, unlike chitinases, these proteins lack chitinase enzymatic activity (Chang et al. 2001). Chi3l3 is normally produced in alveolar and splenic macrophages, as well as bone marrow myeloid progenitors, and is induced as a result of inflammation or tissue injury (Nio et al. 2004). While the exact function of this protein remains unknown, it is thought to possibly play a role in host immune defense since, as a chitinase-like protein, it has the ability to bind pathogens containing chitin, such as fungal and parasitic organisms, including *Pneumocystis spp.* (Guo, Johnson, and Schuh 2000), *Cryptococcus spp.* (Feldmesser, Kress, and Casadevall 2001), and invasive nematodiasis (Sato et al. 1988; Takamoto et al. 1997). As such, crystalline material within these lesions also stains reddish-orange with Luna stain, which is known to bind to chitin (Figure 1H). Chi3l3 is also expressed during a variety of inflammatory responses due to traumatic or chemical stimuli such as particulates and tobacco smoke (Hung et al. 2002). Further, Chi3l3 is thought to play a role in mediating cell–cell and cell–matrix interactions, including those associated with tissue damage, repair, and remodeling because it binds various polysaccharides and glycosaminoglycans involved

in extracellular matrix remodeling and tissue repair (Nio et al. 2004; Waern et al. 2010). Other investigators have postulated that it may contribute to hematopoiesis, since it is expressed in the fetal liver and adult hematopoietic tissue including the spleen and bone marrow and has been associated with crystal formation in a mouse model of myeloid leukemia (Marchesi et al. 2003).

In summary, aberrant expression of the target gene in this transgenic mouse model was associated with marked pulmonary disease consistent with ECP. This disease is associated with overexpression of Chi3l3 protein, leading to the influx of dense macrophage and multinucleate giant cell infiltrates containing fine intracellular to large angular extracellular crystalline material. This lesion is unique in the mouse and may be influenced by strain, genotype, or concurrent disease. While this lesion was most certainly influenced by the transgene in these mice, it remains a good example that, as with all genetically modified mice, familiarity with background strain-related lesions is critical in making sense of various observed phenotypes that otherwise may be attributed to genetic modification.

Adrenal Cortical Lesions

A presentation on adrenal cortical lesions by Dr. Victoria A. Laast (Covance Pharmaceutical R&D Co., Ltd., Shanghai, China) was a collaborative effort with Drs. Gary Boorman and Thomas Larsen (Covance Laboratories, Inc., Chantilly, VA). Three challenging cases were presented to the audience for voting to address features of cortical degenerative and proliferative lesions. All three cases were from female Sprague-Dawley rats on a 2-yr carcinogenicity study. The first case depicted a nonencapsulated, uncircumscribed lesion that involved the cortex on one side of the adrenal gland. A series of low and higher magnification images showed that the lesion consisted mainly of vacuolated cells within the zona fasciculata, separated by small cystic spaces filled with proteinaceous material (Figure 2A–C). Voting choices made available to the audience were (1) focal cortical hyperplasia, (2) cortical vacuolation, (3) cortical cystic degeneration, (4) cortical adenoma, (5) cortical adenoma with vacuolation, (6) focal hyperplasia, and (7) other. Cortical cystic degeneration was the speaker's preferred choice and received 48% of the votes. However, other votes recorded were cortical adenoma with vacuolation (23%), cortical adenoma (11%), cortical vacuolation (7%), focal cortical hypertrophy (4%), focal cortical hyperplasia (3%), and other (3%).

The second case was also cortical cystic degeneration but with a different presentation from the first case. At necropsy, the adrenal gland was grossly dark red and enlarged. Microscopically, the lesion was well circumscribed but nonencapsulated with minimal compression of adjacent parenchyma. The lesion was contained mainly within the zona fasciculata, with atrophy and vacuolation of cells in the zona glomerulosa. Cells within the lesion were slightly hypertrophied, several of which had vacuolated cytoplasm. Cystic spaces were present within the lesion (Figure 2D–G). The voting choices and results were (1) cortical angiectasis (4%), (2) cortical vacuolation (9%), (3) cortical cystic degeneration (14%), (4) focal cortical hypertrophy (14%), (5) cortical adenoma with vacuolation (57%), and (6) other (1%). The speaker's preferred diagnosis was cortical cystic degeneration and was based on the lack of atypia or lack of disorganization of the cortical cells, presence of

cystic spaces and fewer cells (compared with an adenoma) within the lesion (Figure 2F and G). The audience's preference of cortical adenoma may have been due to the large size of the lesion with compression and atrophy of adjacent parenchyma (Figure 2D). During discussions on this case, the possibility of these lesions being functional was debated based on the atrophy of the contralateral adrenal gland. One participant indicated the preference for the diagnosis of focal cortical hypertrophy based on the presence of hypertrophied cells within the lesion. However to prevent the use of multiple diagnosis when there is prominent vacuolation in the lesion, the speaker recommended using the term cystic degeneration.

The third and last case presented by Dr. Laast was a cortical adenoma (Figure 2H–J). The voting choices and results were (1) focal cortical hypertrophy (2%), (2) diffuse cortical hypertrophy (0%), (3) focal cortical hyperplasia (0%), (4) cortical cystic degeneration (7%), (5) cortical adenoma (73%), (6) cortical carcinoma (18%), and (7) other (0%). The speaker's preferred diagnosis of cortical adenoma was the option favored by the audience. During discussions, this case was compared and contrasted with the second case. In this last case, features of adenoma were the enlarged and increased numbers of cells that were arranged in distorted cords with minimal cellular atypia (Figure 2I). Mitoses were noted in low numbers (Figure 2J).

The discussion then moved to a review of cortical cystic degeneration in the adrenal of rats, from early lesions to well-developed lesions. Cystic degeneration of the adrenal cortex is a common age-related finding in the Sprague-Dawley strain, occurring more frequently in female rats. Compression of adjacent cortex, a common hallmark of benign adrenal cortical tumors, often accompanies foci of cystic degeneration creating a diagnostic dilemma. Certain stages of cystic degeneration with an atypical presentation, as in the second case, tend to present a diagnostic challenge. Accurately differentiating these relatively common degenerative changes from proliferative lesions is critical in safety assessment studies. Cystic degeneration appears to arise in the zona fasciculata of the adrenal cortex, often causing compression along part of the margin of the lesion. The degenerating cells are large with abundant eosinophilic cytoplasm or contain clear cytoplasmic vacuoles (McMartin et al. 1992; Brix et al. 2005). Mitotic figures are generally uncommon (Hamlin and Banas 1990). In contrast, adrenal cortical hyperplasia and adrenal cortical adenoma are frequently comprised of smaller cells causing compression. Mitotic figures can often be found. Cytological details and growth patterns (increase in number of cells in hyperplasia and adenomas vs. decrease in number of cells and/or hypertrophy of cells in cystic degeneration) are more useful criteria than compression for separating degenerative from proliferative lesions in the adrenal cortex of Sprague-Dawley rats.

Atypical Foci of Altered Hepatocytes

Dr. Susan Elmore (NTP, NIEHS, Research Triangle Park, NC) presented an unusual liver lesion from an as yet unpublished NTP chronic dosed water toxicity and carcinogenicity bioassay. In addition to the pathology working group (PWG), the pathologists involved in the review of these studies include the NTP pathologist (Dr. Abraham Nyska, Integrated Laboratory Systems, Inc. Consultant, RTP, NC), the study pathologist (Dr. Anthony Skowronek, Battelle Memorial Institute, Columbus, OH), the QA pathologist (Dr. Holly

Kolenda-Roberts, EPL, RTP, NC), and the PWG pathologist (Dr. Crystal Johnson, Charles River Laboratories, PAI, RTP, USA).

Male and female B6C3F1 mice were dosed via water for either 52 weeks (interim sacrifice) or 105 weeks (terminal sacrifice). The audience viewed a series of low- and high-magnification images of focal liver lesions with atypical hepatocytes (Figure 3A–D). The majority of the voting attendees (71%) chose either focus of hypertrophied hepatocytes, cellular atypia (37%) or focus of cellular alteration, atypical (34%). The other available diagnoses garnered from 2% to 8% of the votes: focus of hyperplastic hepatocytes, cellular atypia (8%), focus of cellular alteration (7%), hepatocellular dysplasia (5%), hepatocellular carcinoma (4%), hepatocellular nodular hyperplasia (4%), and hepatocellular adenoma (2%).

These unusual lesions had features that were only identified within what were considered to be eosinophilic or mixed cell foci (Figure 3E). This particular characteristic was difficult to portray within a few select images for voting and may have resulted in the split vote. These lesions were either single or multifocal foci of altered hepatocytes with markedly enlarged hepatocytes that merged with the surrounding parenchyma or occasionally caused slight compression (Figure 3F and G). The borders were sometimes irregular as seen in Figure 3C. The hepatocytes within the foci had either solid eosinophilic cytoplasm or contained multiple small discrete clear vacuoles (i.e., microvesicular vacuolation; Figure 3H–K). There was marked cellular atypia with anisocytosis, karyomegaly, multiple prominent nucleoli, and single or multiple intranuclear eosinophilic invaginations (Figure 3L). The incidences for this lesion in the 1- and 2-yr studies are presented in Table 1.

This lesion was not present in the 13- or 26-week mouse studies and was not present in rats. In the 1-yr study, the lesions were generally smaller and did not contain the clear cytoplasmic vacuoles seen in the 2-yr study. The PWG that was convened to evaluate these studies considered the diagnosis and pathogenesis of this lesion with much discussion and debate. One term that was considered was "eosinophilic or mixed cell focus, atypical" since these lesions appeared to arise within foci of altered hepatocytes. Another term that was considered by the PWG was "hepatocellular dysplasia" since they contained similar morphologic features of the potentially preneoplastic human liver lesion. But, in humans, hepatocellular dysplasia is a peculiar pattern of hepatocellular proliferation mainly observed in cirrhotic nodules in patients with hepatocellular carcinoma (Pollice et al. 1988). Adenoma and carcinoma were terms also considered by the PWG but were not used because these unusual lesions lacked these features; distinct compression or invasion of surrounding parenchyma, hepatic plates impinging at sharp angles to the surrounding parenchyma, necrosis, hemorrhage, abnormal growth pattern, metastases (Table 2; Harada et al. 1999). On the other hand, these lesions had most of the features of foci of altered hepatocytes but also had marked cellular atypia (Table 2). Moreover, the animals in this study also developed morphologically typical adenomas and carcinomas without cellular atypia as a major component. One term that was considered was "hyperplasia, atypical, focal" due to the similarities to liver lesions from mice treated with dioxin-like compounds. However, the lesions from the studies of dioxin-like compounds lacked the marked atypia seen in this study. Also, the lesions in this study did not show an increase in cell number but rather an

increase in cell size. Hepatocellular nodular hyperplasia was also considered by the NTP, but in rodents this term defines a specific regenerative lesion that is seen in response to liver injury. The lesions seen in this study did not appear to occur secondary to liver injury and lacked hyperplasia. After much consideration and debate, the final NTP term used for this lesion was "focus of altered hepatocytes, atypical."

The preliminary results from the yet to be published 1-yr bioassay show treatment-related statistically significant increased incidences of hepatocellular carcinomas (including multiples) and hepatoblastomas (including multiples) in male and female mice. However, hepatocellular adenomas and foci were not significantly increased. Preliminary results from the 2-yr bioassay show treatment-related statistically significant increased incidences of hepatocellular carcinomas (including multiples), hepatoblastomas (including multiples), and hepatocellular cholangiocarcinomas. As in the 1-yr study, hepatocellular adenomas and foci were not significantly increased.

A search of the more than 570 chemical bioassays in the NTP database revealed only 4 other NTP studies reported hepatocyte karyomegaly, and all were considered to be hepatocarcinogens based on treatment-related increased incidences of neoplasia: 2-Methylimidazole (TR-516), Chloramine, and two Pentachlorophenol Technical-Grade Mixtures (TR-349). However, the karyomegaly was present in scattered hepatocytes within the parenchyma and did not occur within foci. Thus, to date, this is the only lesion of this type identified in NTP studies, and we are unaware of such lesions being reported in the literature.

The hepatocellular atypia seen in this study may be preneoplastic and may transition to carcinoma, but if so, it is not understood why the carcinomas in this study do not display the marked cellular atypia as seen within these foci. Also, if this lesion is preneoplastic, then why is it not seen in other chronic studies of hepatocarcinogens? Further investigation into the pathogenesis of this unusual lesion is warranted.

Cardiac Schwannoma versus Cardiomyopathy

Dr. Michael Boyle (NTP, NIEHS, Research Triangle Park, NC) presented four cases involving cardiac tissue. These four cases were among several that were the subject of a PWG at the NTP from a 2-yr oral gavage carcinogenicity bioassay in male and female Fischer 344/N rats. Some of these examples were brought to the attention of the NTP by Dr. Kevin Isaacs. Dr. Boyle indicated before the voting block that, despite the name of the case series, not all diagnoses necessarily incorporated a Schwann cell origin. The audience was presented with the following options: (1) cardiomyopathy, (2) fibrosis, (3) Schwann cell hyperplasia, (4) schwannoma, (5) benign schwannoma, (6) malignant schwannoma, (7) atriocaval mesothelioma, or (8) other. Several images of the first case, a myocardial lesion from a male rat, were shown at escalating magnifications. The majority of participants (54%) voted for “cardiomyopathy” as the preferred diagnosis, followed by 24% for “fibrosis” and 14% for “Schwann cell hyperplasia.” The lesions consisted of a locally extensive region of cardiomyocyte necrosis and replacement by fibrosis and mononuclear infiltrates including pigmentladen macrophages (Figure 4A). Remaining cardiomyocytes

multifocally contained variably sized sarcoplasmic vacuoles. The lesions observed were consistent with what is commonly known as “rodent progressive cardiomyopathy,” which was the consensus diagnosis for this and similar lesions at the NTP PWG (Greaves 2007; MacKenzie and Boorman 1990). Dr. Boyle pointed out that later presentations and efforts by the INHAND Cardiovascular Organ Working Group were seeking to update and clarify nomenclature as it pertains to the diagnosis of cardiomyopathy.

The second case consisted of a series of images from a female rat showing a subendocardial lesion that extended into, expanded, and subtotally obliterated the papillary muscle and several adjacent chordae tendinae. Again, a plurality of participants (50%) favored a single diagnosis of “schwannoma” for this lesion, while 22% preferred a diagnosis of “benign schwannoma.” The lesion consisted of a mildly anisocytotic and anisokaryotic subendocardial spindle cell proliferation that spanned the endocardium, visible in the photomicrograph from the apical endocardium to the basilar endocardium (Figure 4B). The spindle cell proliferation was approximately 20 to 30 cell layers thick in this zone and was predominantly arranged in orderly streams multifocally interrupted by haphazard bundles. This proliferation extended into the papillary muscle, where additional morphologies were observed. The proliferation exhibited whorling and packeting behavior with palisading of nuclei and increased cellular density in some areas (Antoni A-type) and decreased cellular density with increased intercellular matrix (Antoni B-type) in others. Multifocally, increased anisocytosis and anisokaryosis were observed. Dr. Boyle informed the group that the PWG concurred with the diagnosis of schwannoma for this lesion, and that this lesion was typical of the endocardial presentation of schwannomas seen in this and other studies (Alison et al. 1987; MacKenzie and Boorman 1990).

Three images from the third case from a male rat showed increasingly higher magnifications of an intramural infiltrative lesion within the middle third of the right ventricle. The lesion consisted of interwoven bundles of neoplastic spindle cells that replaced and displaced nascent cardiomyocytes (Figure 4C). The neoplastic cells were mildly anisocytotic and anisokaryotic. Entrapped cardiomyocytes exhibited the necrotic and degenerative phenotype observed in the first case; however, the prominent inflammatory cell infiltrate and fibroplasia was not observed in this lesion. Multifocal cardiomyocytes within the lesion exhibited an Anitschkow cell-type chromatin pattern, with nuclear material arranged in a centralized bar within the nucleus. The myocardium immediately surrounding the advancing edge of this lesion was unaffected. A narrow margin of participants favored a diagnosis of schwannoma (26%) for this lesion, followed by fibrosis (25%) and “malignant schwannoma” (18%). The NTP PWG diagnosed this lesion as a schwannoma. Dr. Boyle indicated this lesion was representative of the typical intramural schwannoma seen in this and other studies, but that the varying audience interpretations were informative (Greaves 2007; MacKenzie and Boorman 1990).

The fourth and final case was represented by a series of increasing magnifications of a lesion that affected the outer third of the ventricle in a male rat. The lesion consisted of a regionally extensive spindle cell proliferation that dissected and displaced cardiomyocytes in this zone (Figure 4D). These cardiomyocytes predominantly appeared nondegenerate, although degenerate myofibers were present multifocally. Multifocal cardiomyocytes contained

slightly basophilic cytoplasm and multiple karyomegalic nuclei, indicating a regenerative effort. When the voting was tallied for this lesion, 38% of participants favored fibrosis, while 25% favored cardiomyopathy, followed by 15% for Schwann cell hyperplasia and 13% for malignant schwannoma. The NTP PWG consensus for this lesion was cardiomyopathy.

Dr. Boyle continued the presentation by stating that the lesions from all four cases represented a spectrum of background lesions and that much discussion during the PWG focused on the schwannoma criteria for diagnosis and terminology. Regarding the second and third cases, which were representative of several of the more than 20 proliferative cardiac lesions, it was decided that a diagnosis of schwannoma would be used. Based on the low incidence of these lesions, the lack of knowledge of their biologic behavior, and the reported metastasis of seemingly benign schwannomas, it was decided by the PWG that the diagnoses benign schwannoma and malignant schwannoma would not be used (MacKenzie and Boorman 1990; Teredesai and Woehrmann 2005). Canonical diagnostic criteria for purported Schwann cell lesions were discussed, as was the question of differences between endocardial and intramural schwannomas, and the issue of distinguishing benign from malignant tumors (Alison et al. 1987; Novilla et al. 1991). Dr. Boyle outlined an investigation planned at the NTP, which included review of the morphology of all varieties of schwannomas, including those diagnosed as malignant, benign, “not otherwise specified” (NOS), endocardial, and intramural. The planned immunohistochemical (IHC) investigation to elucidate the differentiation of these lesions, including S-100 (Schwann cell, neural crest) and epithelial membrane antigen (EMA, perineural), was also discussed by the PWG (Hornick, Bundock, and Fletcher 2009; Langford, Porter, and Bunge 1988; Nagatani et al. 2009; Nikitin et al. 1991).

The topic of diagnosing the purported cell proliferative lesions as solely schwannomas as opposed to benign schwannoma or malignant schwannoma generated considerable audience discussion. Lacking knowledge of the biology and true origin of these tumors, coupled with the potential for morphologically benign tumors to behave malignantly, the term schwannoma (without a benign or malignant designation) was preferred by most participants at the PWG (Novilla et al. 1991).

Cardiac Papillary Muscle Lesions

In this presentation, Dr. Matthias Rinke from Bayer Pharma AG showed some alterations of the cardiac papillary muscles from male and female Beagle dogs. The samples were taken from different bioassays (4 weeks to 12 mo) with animals aged between 6 mo and 2 yr.

Case 1 represented the normal features of a left ventricular papillary muscle which was correctly diagnosed by the vast majority of the audience (88%). Focal fibrotic strands within a normal myocardium did not represent a pathologic condition but showed the normal insertion sites of the chordae tendinae.

Case 2 showed a small (acute) focal myocardial necrosis lesion of the papillary muscle located close to the insertion site of the chordae tendinae (Figure 5A). This was characterized by early hyaline fiber degeneration and acute necrosis with increased numbers

of sarcolemmal nuclei. Voting choices and results were normal (10%), focal necrosis (5%), focal myocardial necrosis (17%), focal myocardial necrosis of the papillary muscles (3%), focal acute myocardial necrosis of the papillary muscles (14%), and other, for example, artifact (51%). Approximately half of the voting participants considered this lesion an artifact and another 10% thought it to be normal. The diagnosis of artifact/normal is not surprising in this case, given the similarity to commonly observed postmortem artifacts (i.e., myocardial eosinophilia and shrunken fibers) and the difficulty to differentiate from acute necrosis (Kemi et al. 1995). This case illustrates the need for the pathologist to have complete information (i.e., chemical, dosing regimen, necropsy protocol, postnecropsy tissue handling, dose effects, etc.) in order to make an accurate diagnosis.

Dr. Rinke showed a series of pictures demonstrating the timely progression of the lesion, which started shortly after a single treatment with a dihydropyridine. The pathogenesis of this lesion involves acute focal hypoxia/anoxia of the musculus papillaris subauricularis or musculus papillaris subatrialis, resulting in infiltration of inflammatory and regenerative cells (Figure 5B). Grossly these lesions present as red to grayish subendocardial foci. Clinically one may observe tachycardia and extrasystoles, especially in heavier animals. Comparable cardiovascular lesions in dogs were first described by Luginbühl and Detweiler in 1965. In 1969, Balazs et al. described papillary muscle necrosis after administration of large doses of isoproterenol, a well-known compound used to lower blood pressure. The term myocardial papillary muscle necrosis in dogs was introduced by Balazs and Payne in 1971, after administration of hypotensive compounds and has since been cited in some medical textbooks as the "Balazs phenomenon." However, the name Balazs was only familiar to 10% of the audience. During the discussion the question was raised as to whether a very recently published report on myocardial toxicity in a group of greyhounds could be related to the same mechanism (Yaeger et al. 2012). Dr. Rinke was not yet aware of this article but assumed that it might be possible, especially in a dog breed trained for high performance under extreme oxygen need. However, by reviewing the article it became clear that in this collective of dogs, the myocardial toxicity showed a later onset and was also accompanied by arterial and skeletal muscle damage, a condition that was never reported in the cases presented herein.

Case 3 was an example of a spontaneous lesion of extended focal myocardial fibrosis with areas of mineralization (Figure 5C and D). The voting choices and results were focal myocardial fibrosis (7%), chronic myocardial fibrosis (5%), focal chronic myocardial fibrosis (9%), subacute focal myocardial fibrosis, (1%), focal myocardial fibrosis with mineralization (77%), and other (1%). While the lesion was recognized by nearly all voting participants, the more precise description of “focal myocardial fibrosis with mineralization” was chosen by the majority. One participant noted that such lesions are occasionally observed as background findings. Dr. Rinke pointed out the importance of determining the age of a lesion and dose response in order to avoid misinterpretation with an induced alteration.

The presentation concluded with an example of induced myocardial fibrosis of the left ventricular papillary muscles, which had been observed in a 1-yr dog study using an agrochemical compound. In this study, there was a dose-dependent increased incidence and

severity of areas with replacement fat and fibrosis (mature collagen fibers; Figure 5E and F). Dr. Rinke explained the different approaches they had taken to evaluate to a no adverse effect level, knowing that this kind of lesion may also arise in controls. He suggested that accurate evaluation and diagnosis should involve additional step sections and special stains (e.g., Goldner), lesion localization within the left ventricle (i.e., musculus papillaris subauricularis or musculus papillaris subatrialis), and implementing a precise grading scheme according to size, multiplicity, and location within the muscle.

Pancreatic Ductal Cell Lesion

Dr. Katsuhiko Yoshizawa of Kasai Medical University presented an unusual pancreatic lesion from a 21-day-old female LEWIS rat that was injected once intraperitoneally at birth with 35 mg/kg *N*-methyl-*N*-nitrosourea (MNU). This lesion was a solitary nodule, approximately 500 × 600 mm in length, with encapsulation and slight compression of the surrounding tissue (Figure 6A). It was characterized by ductal structures composed of cells with large nuclei and scant cytoplasm, without zymogen granules (Figure 6B). No necrotic areas or inflammation were present within this nodule. Mitoses and expansion of the lesion, combined with proliferating cell nuclear antigen (PCNA)-positive cells, confirmed the proliferative nature of this lesion (Figure 6C). Some scattered surrounding acinar cells were also positive for PCNA, indicating that these acinar cells have some normal proliferative activity at the age of 21 days.

To confirm the origin of this nodule, various IHC markers were used; pan-cytokeratin (CK) for pancreatic duct cells; amylase for acinar cells; and insulin and pancreatic and duodenal homeobox 1 (PDX-1) for islet cells. PDX-1 is a transcription factor necessary for β-cell maturation and is expressed in the normal islet cells of adult rats (Hosotani et al. 2004). The results of the IHC showed that the cytoplasm of cells within this nodule was positive for CK as well as the surrounding normal ductal cells (Figure 6D). Although there was also some very weak staining in the surrounding acinar cells, this appeared to be background staining. The IHC for alpha-amylase revealed that no signal was seen in the cytoplasm of cells within this nodule (Figure 6E). On the other hand, the cytoplasm of normal acinar cells was strongly positive for amylase. Immunohistochemistry for insulin (Figure 6F) and PDX-1 revealed no signals in the cytoplasm of cells within this nodule. However, as an internal positive control, islet cells were positive for insulin and PDX-1. Based on the results of the IHC analyses, the inmmunoreactivity in this nodule was similar to ductal cells, suggesting the origin was “ductal cell.”

After viewing only the hematoxylin and eosin (H&E) images, the voting choices and results for this lesion were islet cell hyperplasia (2%), islet cell adenoma (13%), acinar cell hyperplasia (14%), acinar cell adenoma (28%), ductal cell hyperplasia (10%), ductal cell adenoma (32%), and regeneration (1%). Forty-two percent felt that it was of acinar cell origin and 42% felt that it was of ductal cell origin. The discussion points were whether this lesion is nonneoplastic or neoplastic, whether this lesion is of islet, acinus, or ductal origin, and whether this lesion is spontaneous occurring or MNU induced. After presentation of the results of the IHC analyses, most audience members agreed that this nodule was a benign

tumor and that the origin was ductal cell. Some audience members felt that this lesion was a malignant tumor because of the high proliferative activity.

Table 3 compares and contrasts the criteria for proliferative lesions of pancreatic ducts (Hansen et al. 1995; Riley et al. 1990; goRENI, http://www.goreni.org/). This lesion was an encapsulated nodule with proliferative activity that showed compression of the surrounding tissue without invasion and cellular atypia. Therefore, this nodule is most likely a benign ductal tumor. During subsequent discussion, the possibility was raised that this lesion may be a developmental anomaly. MNU is a direct-acting alkylating agent that interacts with DNA and accumulation of mutations enhances cancer risk in the pancreas of several animal species. MNU induces acinar cell adenocarcinoma in guinea pigs and mice (Reddy and Rao 1975), while mainly inducing ductal cell adenocarcinoma in the Syrian golden hamster (Furukawa et al. 1992). In contrast, in the case of rats, MNU mainly induces acinar cell hyperplasia and rare cases show progression to cancer (Monis et al. 1991). Therefore, this lesion is most likely induced by MNU. However, we cannot rule out the possibility of a developmental anomaly since tissues were not evaluated prior to treatment with MNU.

Intrahepatocytic Erythrocytes and Subendothelial Hepatocytes

Dr. Linda Kooistra and Dr. James Morrison (Charles River Laboratories, Pathology Associates, Durham, NC), in collaboration with Dr. Susan Elmore (NIEHS/NTP) and Dr. Robert Maronpot (Maronpot Consulting, LLC), presented two cases of unusual liver lesions in rodents. The first case was from a B6C3F1 mouse in a 280-day NTP Immunotoxicity oral gavage study. After presentation of several images (Figure 7A–D) of liver tissue, which contained abnormal accumulations of red blood cells, a vote was taken. The voting choices and results were artifact (1%), angiectasis (1%), emperipolesis (9%), erythrophagocytosis (25%), intrahepatocytic erythrocytes (22%), hepatic erythrophagocytosis (33%), hepatocyte cytoplasmic inclusions (9%), and other (0%). The NTP diagnosis was “intrahepatocytic erythrocytes.” In previous NTP studies, this lesion had been recorded as hepatic erythrophagocytosis.

After the vote, Dr. Kooistra showed transmission electron micrograph images (Figure 7E and F) of the lesion. It was noted that the red blood cells did not appear to be confined by a lysosomal membrane. The lack of a lysosomal membrane around the red blood cells eliminated both macrophage and hepatocyte-mediated erythrophagocytosis as differential diagnoses. The red blood cells were also clearly within the cytoplasm of the hepatocyte and not within endothelial lined spaces, thereby eliminating angiectasis as a differential. Emperipolesis is the active penetration of one cell by another cell and both cells remain viable. Emperipolesis differs from phagocytosis in that with emperipolesis the cell enters by an active process, remains viable, and can exit again with no damage to either cell. It is difficult to ascribe an active process to red blood cells invading hepatocytes as red blood cells lack the cellular structural components or a nuclear command center to orchestrate such a movement. “Hepatocyte cytoplasmic inclusions” is a possible diagnosis but does not directly address the fact that the inclusions are red blood cells. Therefore, intrahepatocytic erythrocytes (i.e., intrahepatocellular erythrocytes) was considered the most appropriate diagnosis by the NTP.

Histologically the lesion is characterized by the presence of one to many red blood cells within the cytoplasm of enlarged hepatocytes. Often the hepatocyte nucleus is centrally located with slightly condensed chromatin. In hepatocytes that contain many red blood cells, the hepatocyte cytoplasm is often pushed peripherally to form a circular rim of cytoplasm against the cell membrane. The cytoplasm of other adjacent hepatocytes is often of decreased density.

This lesion generally appears to be treatment related although a few cases have been seen in controls. It has been seen in both male and female rats and mice and in both short-term and long-term studies (Tables 4 and 5). The significance and method of movement of erythrocytes from the extracellular space through the hepatocyte cell membrane remain unknown.

Dr. James Morrison presented the next case, which was a lesion that occurred in high incidence in the liver of B6C3F1 mice that had been treated with Pulegone in a 2-yr chronic gavage study (TR 563: http://ntp.niehs.nih.gov/ntp/htdocs/LT_rpts/TR563.pdf). After presentation of several images (Figure 7G–J), a vote was taken. The voting choices and results were vascular pseudoinvasion (4%), intravascular hepatocytes (17%), venous intramural hepatocytes (23%), vascular infiltration of hepatocytes (6%), metastatic hepatocellular carcinoma (0%), extension of perivascular focus of cellular alteration (0%), or other (50%). The NTP PWG diagnosis was “intravascular hepatocytes,” a choice based on the recommended use of this term for this lesion in the INHAND: Proliferative and Nonproliferative Lesions of the Rat and Mouse Hepatobiliary System guidelines (Thoolen et al. 2010).

Dr. Morrison showed IHC-stained slides (Figure 7K–P) and trichrome-stained slides (Figure 7Q–R) of the lesion to further illustrate the position of the hepatocytes within the venous wall. The CD31 and factor 8-related antigen antibodies both target endothelial cells (Figure 7K–N). These markers reveal that the hepatocytes are covered by a layer of endothelial cells. The smooth muscle actin IHC stain (Figure 7O and P) and the trichrome special stain (Figure 7Q and R) identified remaining portions of the fibromuscular vein wall. The hepatocytes were clearly between the thin fibromuscular vein wall and the endothelium of the lumen. In some areas, the hepatocytes were noted to be migrating from the hepatic parenchyma through the remaining fibromuscular tissue of the venous wall as illustrated with the trichrome stain (Figure 7S and T).

Fifty percent of the audience members chose “other,” with no majority preference for the other voting choices. During discussions, the audience suggested that the term subendothelial hepatocytes would be a more accurate diagnostic term than intravascular hepatocytes as the term intravascular generally refers to cells within the lumen of vessels, and in this case the hepatocytes are clearly beneath the vessel endothelium. A vote was taken on which term the audience preferred and the vote was in favor of using the term subendothelial hepatocytes for this lesion.

The lesion subendothelial hepatocytes is a rare finding. In the chronic NTP Pulegone study, the incidences in male and female B6C3F1 mice were 3/50, 1/50, 15/50, 47/50, and 0/49,

2/50, 20/50, 46/50, respectively. Although there was a high incidence in this chronic NTP Pulegone study, this lesion has not been recorded in previous NTP studies. A previous report in diethylnitrosamine-treated mice noted this lesion within basophilic foci, which extended to incorporate a central vein (Goldfarb et al. 1983; Koen, Pugh, and Goldfarb 1983). In the present case, the subendothelial hepatocytes were not associated with basophilic foci. In addition to this lesion, there were a number of other significant findings in the livers in this Pulegone study including clear cell, eosinophilic and mixed cell foci, focal and diffuse fatty change, centrilobular hypertrophy, oval cell hyperplasia, bile duct hyperplasia, bile duct cysts, necrosis, inflammation, pigmentation, hepatoblastomas, hepatocellular adenomas, and hepatocellular carcinomas. However, the lesion of subendothelial hepatocytes (i.e., intravascular hepatocytes) was not directly located within or associated with these other various lesions in the liver.

In summary, the important findings of this lesion are: (1) usually involves medium to large size hepatic veins, (2) hepatocytes protrude into the vein lumen and infiltrate the vein wall, (3) infiltrating hepatocytes are covered by an endothelial cell lining, (4) rarely seen in control or treated mice, and (5) not necessarily within basophilic foci or associated with other hepatic lesions. The significance and pathogenesis of this lesion remains unknown.

Pituitary: Lesions of Rathke's Cleft and Pars Distalis

Dr. Deepa Rao (Integrated Laboratory Systems, Inc., RTP, NC) presented some diagnostically challenging lesions in the pituitary gland. This was a project conducted in collaboration with Dr. Rodney Miller (Experimental Pathology Laboratories, Inc., RTP, NC, USA). Dr. Rao first presented a brief overview of the normal pituitary to indicate the location of Rathke's cleft between the pars intermedia and the pars distalis. This was followed by signalment and photomicrographs (Figure 8A-C) from one high-dose group female F344/N rat in a chronic 2-yr NTP bioassay at terminal sacrifice. Voting choices and results were Rathke's cleft: hemorrhage (5%); Rathke's cleft: cyst, hemorrhage (1%); Rathke's cleft: dilatation, hemorrhage (9%); Rathke's cleft: cyst, hemorrhage, sterol clefts (60%); and other (11%). During her presentation, Dr. Rao clarified the terms "dilatation" and "cyst" for the audience. Dilatation is defined as the widening of the space between the pars distalis and the pars intermedia, whereas a true cyst is lined by ciliated cuboidal or columnar epithelium (Lansdown and Grasso 1971; Watanabe 1991). To confirm hemorrhage, a photomicrograph of the lesion under fluorescence was shown to demonstrate the presence of autofluorescing red blood cells in Rathke's cleft. Dr. Rao continued the presentation with signalment and photomicrographs (Figure 8D-F) from another high-dose group female F344/N rat from the same study. Voting choices and results for the second set of photomicrographs were pars distalis: macrophage, pigment (15%); pars distalis: hypoplasia (1%); pars distalis: atrophy (1%); pars distalis: hypoplasia; macrophage, pigment (13%); pars distalis: atrophy, macrophage, pigment (70%); and other (1%). During her presentation, Dr. Rao described the lesion for the second case as small focal areas "capping" Rathke's cleft and the pars intermedia, showing cell loss and stromal collapse, most likely due to necrosis (photomicrographs of extensive necrosis in the pars distalis were shown). Often, these areas contained infiltrates of histiocytes, most likely filled with hemosiderin

pigment. The lesions noted were treatment and dose related in the chronic studies with α,β-Thujone (NTP, 2011, TR570).

Dr. Rao continued her presentation with a brief overview of Rathke's pouch, Rathke's cleft, and the development of the pituitary gland. In humans, Rathke's cleft is reduced to a small series of fluid-filled cysts, with no known functional significance. During development of the pituitary gland, an evagination (Rathke's pouch) from the dorsal surface of the oral cavity toward the brain abuts a downward vesicle from the floor of the brain toward the oral cavity. Eventually, the evagination forms the adenohypophysis and the vesicle forms the neurohypophysis. The adenohypophysis consists of the pars distalis, pars tuberalis, and the pars intermedia. The pars distalis and pars tuberalis originate from the anterior wall of Rathke's pouch, while the pars tuberalis comes to form a sort of sleeve-like covering of the infundibular stalk. The pars intermedia arises from that portion of the wall of Rathke's pouch, which initially is in close proximity to the brain vesicle. The lumen of Rathke's pouch persists in the adult rat as a cleft or potential space between the pars intermedia and pars distalis (MacKenzie and Boorman 1990). Dr. Rao then continued her presentation to delineate types of cysts in the pituitary including congenital cysts, degenerative cysts, craniopharyngeal cysts, and pseudocysts. Congenital cysts are usually due to the persistence of Rathke's pouch or remnants; degenerative cysts are frequently found in the pars distalis in older rats (>1 yr) and should be differentiated from angiectasis or collections of protein-rich fluid in vascular spaces; craniopharyngeal cysts are located around the pituitary stalk and pars tuberalis; and pseudocysts lack an epithelial lining and are commonly found in the pars distalis of aging rats.

Discussion with the audience centered on the etiology of the lesion with suggestions that it may have been of vascular origin. Dr. Rao concurred and elaborated on the blood supply to the pituitary indicating that the pituitary does not harbor a typical ductwork of blood vessels, but rather, has a portal arrangement of blood-filled sinuses between cords of functional cells. These blood-filled sinuses may be vulnerable to any compressive force that may lead to ischemia and subsequent necrosis of the pituitary (Daniel and Prichard 1956). Although the morphological diagnoses in both cases were straightforward, solicitation by Dr. Rao to the audience to inquire if anyone had come across this lesion or anything similar did not elicit any response, indicating that the lesion may be rare.

Pernicious and Megaloblastic Anemia

Dr. Michelle Cora (NTP, NIEHS, Research Triangle Park, NC) presented hematology data from B6C3F1 female mice exposed to a compound under study at the NTP. The presentation focused on the erythron and blood smears collected at day 90 (study termination) of the study. Data from the control group and all dose groups were presented with emphasis on the findings in the high-dose group of 1,000 mg/kg (Table 6). Given the following choices:—(1) pernicious anemia; (2) pure red cell aplasia; (3) iron deficiency anemia; (4) anemia of chronic disease; and (5) immune-mediated hemolytic anemia—, the audience was asked to vote for the choice that was most consistent with the erythron changes. The voting was mixed with the correct answer of pernicious anemia receiving 26% of the vote. Pernicious anemia is a form of megaloblastic anemia characterized by a macrocytic normochromic

nonregenerative anemia. The expected erythron changes of the other choices were briefly discussed. Pure red cell aplasia presents with a profound decrease in the red blood cell count and typically normocytic erythrocytes, while iron deficiency is characterized by microcytic erythrocytes. Anemia of chronic disease is normochromic and normocytic, while immunemediated hemolytic anemia is classically hypochromic, macrocytic, and highly regenerative.

Several blood smear photomicrographs from the 1,000 mg/kg dose group were next presented to the audience (Figure 9A–B). Abnormalities identified on the blood smears from this dose group included a mild increase in anisocytosis as well as several erythrocyte morphology changes (i.e., poikilocytes, acanthocytes) and rare basophilic stippling. As a review of common erythrocyte morphology changes, the audience was asked to identify which, out of the following choices, was *not* represented on the smears: (1) microcytes, (2) keratocytes, (3) schistocytes, (4) acanthocytes, (5) Howell-Jolly bodies, and (6) basophilic stippling. Again, answers were mixed, but the majority (30%) of the audience chose the correct answer of keratocytes. While these morphology changes are not specific for a megaloblastic anemia, they are supportive of the disorder. This is especially true of basophilic stippling, which occurs when there are disruptions of normal erythropoiesis (dyserythropoiesis), as is the case with megaloblastic disorders. Other causes or conditions that may cause a dyserythropoiesis with subsequent erythrocytic basophilic stippling include iron deficiencies, lead poisoning, and preleukemic syndromes.

The development of a megaloblastic disorder or anemia is indicative of a disruption in normal DNA synthesis. Cytologic and histologic features of megaloblastic disorders include anisocytosis, poikilocytosis, increased Howell-Jolly bodies, basophilic stippling, multiple nuclei, nuclear fragmentation, and megaloblastic precursor cells, as observed on peripheral blood smears and/or bone marrow preparations (Bain et al. 2001; Evans 2009). Megaloblastic cells are larger than normal hematopoietic precursors with abnormal nuclear chromatin. Their “giant” abnormal appearance is a result of continued cytoplasmic maturation in the face of slowed cell division caused by impaired DNA synthesis. The finding of these cells is a hallmark of megaloblastic disorders, but their identification is not necessarily needed for a diagnosis.

There are several causes of megaloblastic disorders, including derangements of folate and cobalamin (vitamin B12) metabolism, administration of compounds that directly affect DNA synthesis, as well as diseases such as myelodysplastic syndrome. Folate and cobalamin are needed for normal DNA synthesis. In addition to outright folate or cobalamin deficiency, malabsorption syndromes, changes in bacterial gut flora, and altered enterobiliary secretions (intrinsic factor) can all alter folate and cobalamin metabolism (Bills et al. 1992; Evans 2009; Wickramasinghe 2006). Furthermore, certain compounds may directly interfere with their uptake (e.g., colchicine) or inhibit enzymes involved in their normal metabolism (e.g., methotrexate; Evans 2009; Wickramasinghe 2006). Compounds that directly affect DNA synthesis include purine analogues (e.g., azathioprine, 6-mercaptopurine) and pyrimidine analogues (e.g., 5-fluorouracil). The administration of azidothymidine (AZT) or 1,3-butadiene has been shown to cause a nonregenerative macrocytic/megaloblastic anemia in mice by directly affecting DNA metabolism (Irons et al. 1986a, 1986b; NTP 1999, TR469).

The exact mechanism by which the compound in this study caused a megaloblastic anemia has yet to be elucidated.

Challenges in Embryonic Diagnoses

The evaluation of transgenic mouse embryos by veterinary pathologists is increasingly common and presents numerous challenges, given the complex and rapid changes that embryos undergo during development. Dr. James P. Morrison (Charles River Laboratories, Pathology Associates, Durham, NC) presented three cases of central nervous system (CNS) malformations in transgenic mouse embryos of different embryonic ages. Dr. Morrison's first case focused on the hindbrain of an E12.5 (roughly mid-gestation) transgenic mouse on a C57BL/6 background. The first image presented was a frontal section through the developing medulla oblongata, cerebellum, and tectum of the midbrain of a normal E12.5 C57BL/6 mouse, in order to illustrate the normal neuroanatomy at this stage of development (Figure 10A). The next two images for voting were different magnifications from the equivalent area of the transgenic mouse (Figure 10B). The voting choices and results were neuroepithelial dysplasia (79%), holoprosencephaly (7%), exencephaly (4%), craniorachischisis (7%), syringomyelia (1%), and other (1%). The audience overwhelmingly chose neuroepithelial dysplasia as the most appropriate diagnosis and Dr. Morrison agreed. The images displayed disorderly growth with numerous rosettes apparent at higher magnification, which is classic for dysplasia in the developing CNS.

Dr. Morrison's second case focused on the forebrain of an E16.5 transgenic mouse on a C57BL/6 background, which is fairly late gestation. The first image was a frontal section through the forebrain of a normal E16.5 C57BL/6 mouse (Figure 10C). The next image was an equivalent section through the transgenic mouse forebrain. The voting choices and results for case 2 were dicephaly (16%), holoprosencephaly (42%), exencephaly (8%), craniorachischisis (22%), syringomyelia (8%), and other (3%). The most striking feature of this case was the continuous cerebral cortex that crossed the midline (Figure 10D). In the control embryo, the dorsal midline was very well developed, with distinct separation of the two cerebral hemispheres and prominent lateral ventricles. These features were completely lacking in the transgenic embryo, consistent with holoprosencephaly.

The prosencephalon is the most rostral region of the neural tube that divides and ultimately differentiates into the thalamus and two cerebral hemispheres. This division normally occurs fairly early in gestation, approximately E8.5-E9 in the mouse, and its failure to occur in part or in total results in the spectrum of lesions known as holoprosencephaly (literally whole prosencephalon). Holoprosencephaly is the most common forebrain malformation in humans, estimated to occur in 1 in 250 fetuses, but only 1 in 16,000 live births (Geng and Oliver 2009). Although in this example the failure of separation is fairly mild and only affects the dorsal forebrain, in the most severe cases the failure of separation is complete, involving both the dorsal and ventral forebrain, and is accompanied by extensive craniofacial abnormalities, including cyclopia.

The first two cases presented by Dr. Morrison were from embryos that had the same transgenic modification (proprietary information). In addition to the neuroepithelial

dysplasia in the hindbrain and the holoprosencephaly of the forebrain, heterozygous animals developed severe hydrocephalus within the first 2 months of life. The mutated gene has been implicated in ciliogenesis and a probable pathogenesis in these animals involves defective primary and secondary cilia. Primary cilia protrude from the cellular membrane, are nonmotile, and typically measure only 1 to 5 μ in length. By transmission electron microscopy, they have been identified on nearly all eukaryotic cells, including all neurons, and are critical for cellular signaling, particularly during development (Louvi and Grove 2011; Veland et al. 2009; Han and Alvarez-Buylla 2010). Secondary cilia occur on epithelial surfaces and, through their rhythmic movement, are responsible for the transport of fluid, mucus, and other material over the epithelial surface. Ependymal cells lining the brain's ventricular system have numerous secondary cilia and when these are absent or defective, cerebrospinal fluid transport is considerably impaired, resulting in hydrocephalus (Banizs et al. 2005). Although the precise mechanisms remain to be elucidated, the constellation of abnormalities present in these homozygous and heterozygous animals is consistent with a defect in the structure and/or function of both primary and secondary cilia.

To underscore the importance of signaling through primary cilia during neurodevelopment, Dr. Morrison showed an image of a cyclopic lamb and explained that the pathogenesis of that lesion is now known to result from the inhibition by the plant toxin cyclopamine of the signaling protein "smoothened" in the hedgehog-signaling pathway, which is localized to primary cilia. Critically important during development, this signal transduction pathway can also be deranged in certain disease states in adult animals, notably certain neoplasms, and as a result, proteins in this pathway have been the target of drug development (Scales and de Sauvage 2009). A member of the audience commented that a Genentech hedgehog pathway inhibitor (Vismodegib) has shown efficacy in cases of basal cell carcinoma and other neoplasms but also had some unexpected side effects. Patients have reported hair loss and taste changes because the hedgehog-signaling pathway is active in differentiation and proliferation of hair follicles and taste buds.

Dr. Morrison's third case was from an E16.5 C57BL/6 mouse embryo. The first image was a parasagittal section from an age-matched normal embryo (Figure 10E), once again to illustrate the normal neuroanatomy at this age, and the second image was from a transgenic embryo (Figure 10F). The voting choices and results were dicephaly (11%), holoprosencephaly (6%), exencephaly (53%), craniorachischisis (19%), syringomyelia (7%), and other (4%). In this example, the salient histologic features were the presence of neuroepithelium on the dorsal surface of the embryo and the continuity of the ventricular system with the exterior. The features indicate that the neural tube in the cranial region failed to properly close and separate from the surface epithelium, consistent with exencephaly.

Neural tube defects, which include exencephaly, craniorachischsis, and spina bifida, are a common phenotype in transgenic mice and have been reported in over 240 mouse mutants or strains to date. The majority of these mouse mutants develop exencephaly, in contrast to humans, which have a near equal incidence of exencephaly (commonly referred to as anencephaly in human pathology) and spina bifida (Harris and Juriloff 2010). The reasons for this species difference are not known.

There is considerable variability in the spontaneous incidence of exencephaly in mice, with certain strains (e.g., NOD, SELH) having incidences as high as 20%, and so knowledge of the background strain is extremely important. Neural tube closure in mice initiates at three locations and proceeds along the remaining neural tube in a zipper-like fashion. Closures 1 and 3 are invariant between strains in their locations at the cervical–hindbrain boundary and rostral end of the neural tube, respectively. Closure 2 is shifted rostrally from its typical location at the forebrain–midbrain boundary in strains that have a high incidence of spontaneous exencephaly (Copp and Greene 2010). Other strains (e.g. DBA/2) have a very low incidence and are considered resistant to developing exencephaly. In these strains closure 2 is shifted caudally into the developing midbrain. Commonly used strains in toxicologic pathology have a low incidence (<1%) and reportedly a typical location of closure 2 at the forebrain–midbrain boundary.

In conclusion, Dr. Morrison emphasized the importance of having age- and strain-matched controls when performing embryo evaluations and focusing on appropriate fixation and processing since embryos can be very prone to artifacts. Dr. Morrison's talk concluded with an audience member emphasizing the importance of embryo evaluation in biology research and that it should be performed by trained veterinary pathologists. Increasingly, she stated, given our lack of involvement overall as a profession, these evaluations are being performed by the researchers themselves who typically do not have the same breadth of training or experience in comparative pathology.

Cardiovascular Lesions in 10- to 12-Week-Old Sprague-Dawley Rats

The Cardiovascular INHAND Organ Working Group (OWG), represented by Dr. Brian Berridge (GlaxoSmithKline, Raleigh, NC), has a goal to establish guidance for terminology as it relates to proliferative and nonproliferative lesions of the heart and blood vessels in rodents. Past OWG discussions have considered the context of use for many of the common terms described and how their application may influence interpretation and risk assessment of morphologic changes in toxicity studies. This presentation was intended to benchmark current uses of common terms and to prompt discussion that might influence not only the content of the Cardiovascular INHAND monograph but also future applications of these terms. Accordingly, a series of images were shared and indicated to represent morphologic changes in the hearts of 10- to 12-week-old Sprague-Dawley rats that may or may not have been treated with a xenobiotic (i.e., the changes depicted could have been considered to be spontaneous or natural disease). The intent was to define a "context of use" not influenced by the presence of a toxicant.

Cardiomyocyte injury is a common manifestation of toxicity or natural disease in rodents. Necrosis as a lethal form of cardiomyocyte injury is generally considered an adverse change when associated with xenobiotic administration but may also be seen with common background or spontaneous diseases. Morphologically, cardiomyocyte necrosis often exhibits a predictable morphologic chronology that has been well characterized in models of catecholamine hyperpharmacology, allowing pathologists to make some judgment of the "age" of a cardiac lesion (Clements et al. 2010).

Figure 11A depicts a well-circumscribed focus of hyaline cardiomyocyte eosinophilia with a few marginating neutrophilic inflammatory cells within the myocardium. Most respondents recognized this to be a focus of peracute to acute cardiomyocyte necrosis, with 42% suggesting necrosis/inflammatory cell infiltrate as an appropriate morphologic descriptor. A third of respondents (29%) would have included degeneration in their term, suggesting a sublethal stage for the injury depicted. Notably, 14% of respondents would have used the more generic cardiomyopathy as their morphologic term.

Alternatively, Figure 11B is an image of a well-circumscribed accumulation of mixed mononuclear inflammatory cells. Respondent votes for this lesion were more evenly split among three different terms. “Inflammatory cell infiltrate” was selected by 39%, while cardiomyopathy and necrosis/inflammatory cell infiltrate garnered 31% and 27%, respectively. The audience generally recognized this lesion to be a focus of cardiomyocyte necrosis. In this image, most of the necrotic cardiac cells have been phagocytized and replaced with inflammatory cells. This lesion is also widely recognized to be the most common manifestation of rodent progressive cardiomyopathy in a young rat (likely influencing the greater application of the term cardiomyopathy).

Rodent progressive cardiomyopathy is a commonly recognized background disease of laboratory rats and mice (Greaves 2007). This syndrome typically manifests in young rodents as multifocal (most frequently, minimal) accumulations of mixed inflammatory cells that represent the sequelae to necrosis of individual or small clusters of cardiomyocytes. Occasionally, more acute foci of cellular necrosis, as depicted in Figure 11A, can be seen. As a potential source of confusion, these same manifestations are typical of cardiomyocyte necrosis resulting from any source of cellular injury to the heart (e.g., xenobiotic injury). Additionally, there is the potential for a xenobiotic to potentiate or worsen natural forms of cell injury, increasing the severity of lesions that look much like those present in untreated control animals. In this case, “severity” is meant to describe either an increase in the size of small numbers of lesions or increased numbers of focal lesions.

Vacuolar changes in the cytoplasm of cardiomyocytes may present a nomenclature challenge as well. Figure 11C depicts an area of myocardium where a number of individual cardiomyocytes are distorted by clear vacuoles that are irregular in shape and size and might be considered to expand the cellular cytoplasm. In contrast, clear vacuoles present in much greater number in Figure 11D are more consistent in size and shape but appear to have less effect on the overall morphology of the cells. A number of potential morphologic descriptors were offered for these cellular changes that ranged from a simple “vacuolation” to the less specific cardiomyopathy.

Figure 11C is the vacuolar lesion of doxorubicin cardiotoxicity where the cytoplasmic vacuolation is recognized to be sarcoplasmic reticulum dilatation with electron microscopic examination (Van Vleet, Ferrans, and Herman 2002). Respondents to this nomenclature challenge were fairly evenly split between vacuolation (41%) and “degeneration, vacuolar” (46%), reflecting the variability in individual approaches to interpreting morphologic changes of cell injury.

Responses to Figure 11D were more variable with nearly half (48%) of respondents voting for vacuolation but another 41% split between degeneration, vacuolar (19%), “lipidosis” (14%), or degeneration (8%). Participants who voted for lipidosis were likely surprised to learn that, using ultrastructural examination, the vacuolar changes were actually swollen and degenerate mitochondria rather than lipid droplets. These changes were observed in rats given 7 daily oral doses of a proprietary xenobiotic.

Use of consistent terminology that accurately reflects a pathologic process in the heart or any other target organ system is important for a number of reasons. Most reviewers of a toxicology report will never examine the tissues from which the data in that report was generated. Accordingly, the terms we use to communicate the pathologic changes in those tissues are all a reviewer has to consider for his or her own interpretation of the study findings. Also, some reviewers (e.g., clinicians) may have experiential contexts that vary from that of the primary reviewer (e.g., pathologist) such that certain terms mean different things (e.g., cardiomyopathy as a clinical syndrome vs. progressive cardiomyopathy of rodents).

Interpretation of the morphologic changes in a toxicity study often requires differentiation of xenobiotic-induced lesions from background disease inherent in our animal models. Given the limited repertoire of ways any particular cell type or tissue can respond to injury, the morphologic manifestations of xenobiotic-induced injury can easily overlap those that characterize a common background disease. Therefore, not every lesion that looks like a background or spontaneous disease will, in fact, be a result of that process. Terminology that reflects the morphology rather than a presumptive disease process is likely more prudent (e.g., necrosis/inflammatory cell infiltrate vs. cardiomyopathy).

Lastly, considerable effort has been put toward identifying and characterizing a widening array of biomarkers that are useful in both the nonclinical and clinical toxicity testing settings. Biomarkers like cardiac troponins (cTns) are very effective for some forms of cardiac injury and when measured at appropriate times (Berridge et al. 2009; Clements et al. 2010). Accordingly, an accurate communication of the chronologic age and character of cardiomyocyte injury is important for choosing cTns as a biomarker. For example, serum cTn measurement is relevant for lesions like that in Figure 11A but might be less useful for a lesion like myocardial fibrosis or vacuolation without cell necrosis as depicted in Figure 11D.

Acknowledgments

The authors wish to thank Eli Ney of the NIEHS for her unique and creative cover artwork for the symposium handouts as well as for her technical expertise in formatting the speaker’s PowerPoint presentations. Thanks also to both Eli Ney and Beth Mahler of EPL for their assistance with manuscript image preparation and to David Sabio of EPL for assistance during the symposium. Appreciation also goes to Sue Pitsch, Krystle Correll, Tierre Miller, and Maureen Kettering of Association Innovation and Management, Inc. for their valuable help with annual advertising and meeting facilities. Also integral to the success of this meeting was the security provided by William Stoeffler of the Stoeffler Group, LLC. This research was supported (in part) by the Intramural Research Program of the National Institutes of Health (NIH), National Institute of Environmental Health Sciences (NIEHS). This article may be the work product of an employee or group of employees of the NIEHS, NIH; however, the statements, opinions or conclusions contained therein do not necessarily represent the statements, opinions or conclusions of NIEHS, NIH, or the U.S. government.

The author(s) received no financial support for the research, authorship, and/or publication of this article.

Abbreviations

AZT	azidothymidine
Chi3l3	Chitinase 3-like 3
CK	pancytokeratin
CNS	central nervous system
cTns	cardiac troponins
ECP	eosinophilic crystalline pneumonia
EMA	epithelial membrane antigen
INHAND	International Harmonization of Nomenclature and Diagnostic Criteria
MNU	*N*-methyl-*N*-nitrosourea
NIEHS	National Institute of Environmental Health Sciences
NTP	National Toxicology Program
PCNA	proliferating cell nuclear antigen
PDX-1	duodenal homeobox 1
PWG	pathology working group
SCID	severe combined immunodeficient
STP	Society of Toxicologic Pathology

References

Adams ET, Auerbach S, Blackshear PE, Bradley A, Gruebbel MM, Little PB, Malarkey D, Maronpot R, McKay JS, Miller RA, Moore RR, Morrison JP, Nyska A, Ramot Y, Rao D, Suttie A, Wells MY, Willson GA, Elmore SA. Proceedings of the 2010 National Toxicology Program satellite symposium. Toxicol Pathol. 2011; 39:240–66. [PubMed: 21177527]

Alison RH, Elwell MR, Jokinen MP, Dittrich KL, Boorman GA. Morphology and classification of 96 primary cardiac neoplasms in Fischer 344 rats. Vet Pathol. 1987; 24:488–94. [PubMed: 3455078]

Bach U, Hailey JR, Hill GD, Kaufmann W, Latimer KS, Malarkey DE, Maronpot RM, Miller RA, Moore RR, Morrison JP, Nolte T, Rinke M, Rittinghausen S, Suttie AW, Travlos GS, Vahle JL, Willson GA, Elmore SA. Proceedings of the 2009 National Toxicology Program satellite symposium. Toxicol Pathol. 2010; 38:9–36. [PubMed: 20008954]

Bain, BJ.; Clark, DM.; Lampert, IA.; Wilkins, BS. Bone Marrow Pathology. Blackwell Sciences; Oxford, UK: 2001.

Balazs T, Payne BJ. Myocardial papillary necrosis induced by hypotensive agents in dogs. Toxicol and Appl Pharmacol. 1971; 20:442–45. [PubMed: 5132784]

Balazs T, Ohtake S, Cummings JR, Noble JF. Ventricular extrasystoles induced by epinephrine, nicotine, ethanol, and vasopressin in dogs with myocardial lesions. Toxicol and Appl Pharmacol. 1969; 15:189–205. [PubMed: 4185489]

Banizs B, Pike MM, Millican CL, Ferguson WB, Komlosi P, Sheetz J, Bell PD, Schwiebert EM, Yoder BK. Dysfunctional cilia lead to altered ependyma and choroid plexus function, and result in the formation of hydrocephalus. Development. 2005; 132:5329–39. [PubMed: 16284123]

Berridge BR, Pettit S, Walker DB, Jaffe AS, Schultze AE, Herman E, Reagan WJ, Lipshultz SE, Apple FS, York MJ. A translational approach to detecting drug-induced cardiac injury with cardiac troponins: Consensus and recommendations from the Cardiac Troponins Biomarker Working Group of the Health and Environmental Sciences Institute. Am Heart J. 2009; 158:21–29. [PubMed: 19540388]

Bills ND, Koury MJ, Clifford AJ, Dessypris EN. Ineffective hematopoiesis in folate-deficient mice. Blood. 1992; 79:2273–80. [PubMed: 1571542]

Brix AE, Nyska A, Haseman JK, Sells DM, Jokinen MP, Walker NJ. Incidences of selected lesions in control female harlan sprague-dawley rats from two-year studies performed by the National Toxicology Program. Toxicol Pathol. 2005; 33:477–83. [PubMed: 16036865]

Chang NC, Hung SI, Hwa KY, Kato I, Chen JE, Liu CH, Chang AC. A macrophage protein, Ym1, transiently expressed during inflammation is a novel mammalian lectin. J Biol Chem. 2001; 276:17497–506. [PubMed: 11297523]

Clements P, Brady S, York M, Berridge B, Mikaelian I, Nicklaus R, Gandhi M, Roman I, Stamp C, Davies D, McGill P, Williams T, Pettit S, Walker D, Turton J, Bounous D, Dunn B, Hausner E, Herman E, Holt G, Lamb M, Louden C, Mylecraine L, MacGregor J, Reagan W, Roome N, Schultze E, Stoll R, Stonebrook M, Taggert P, Thudium D, Topper M, Wallace K. Time course characterization of serum cardiac troponins, heart fatty acid-binding protein, and morphologic findings with isoproterenol-induced myocardial injury in the rat. Toxicol Pathol. 2010; 38:703–14. [PubMed: 20585145]

Copp AJ, Greene ND. Genetics and development of neural tube defects. J Path. 2010; 220:217–30. [PubMed: 19918803]

Daniel PM, Prichard MML. Anterior pituitary necrosis: Infarction of the pars distalis produced experimentally in the rat. Exp Physiol. 1956; XLI:215–29.

Evans, GO. Animal Clinical Chemistry: A Practical Guide for Toxicologists and Biomadical Researchers. Taylor and Francis Group; Boca Raton, FL: 2009.

Feldmesser M, Kress Y, Casadevall A. Intracellular crystal formation as a mechanism of cytotoxicity in murine pulmonary cryptococcus neoformans infection. Infect Immun. 2001; 69:2723–27. [PubMed: 11254641]

France MP, Muir D. An outbreak of pulmonary mycosis in respiratory burst-deficient (gp91(phox−/−))mice with concurrent acidophilic macrophage pneumonia. J Comp Pathol. 2000; 123:190–94. [PubMed: 11032674]

Furukawa F, Sato H, Imaida K, Toyoda K, Imazawa T, Takahashi M, Hayashi Y. Induction of pancreatic tumors in male Syrian golden hamsters by intraperitoneal *N*-methyl-*N*-nitrosourea injection. Pancreas. 1992; 7:153–58. [PubMed: 1553365]

Geng X, Oliver G. Pathogenesis of holoprosencephaly. J Clin Invest. 2009; 119:1403–413. [PubMed: 19487816]

Goldfarb S, Pugh TD, Koen H, He YZ. Preneoplastic and neoplastic progression during hepatocarcinogenesis in mice injected with diethylnitrosamine in infancy. Environ Health Perspect. 1983; 50:149–61. [PubMed: 6873010]

goRENI. The standard reference for nomenclature and diagnostic criteria in toxicologic pathology. Accessed October 2012. http://www.goreni.org/

Greaves, P. Cardiovascular System. In: Greaves, P., editor. Histopathology of Preclinical Toxicity Studies. Academic Press; New York, NY: 2007. p. 270-333.

Guo L, Johnson RS, Schuh JC. Biochemical characterization of endogenously formed eosinophilic crystals in the lungs of mice. J Biol Chem. 2000; 275:8032–37. [PubMed: 10713123]

Hamlin, MH., II; Banas, DA. Adrenal Gland. In: Boorman, GA.; Eustis, SL.; Elwell, MR.; Montgomery, CA., Jr; MacKenzie, WF., editors. Pathology of the Fischer Rat, Reference and Atlas. Academic Press; San Diego, CA: 1990. p. 501-18.

Han Y, Alvarez-Buylla A. Role of primary cilia in brain development and cancer. Curr Opin Neurobiol. 2010; 20:58–67. [PubMed: 20080044]

Hansen, JF.; Ross, PE.; Makovec, GT.; Eustis, SL.; Sigler, RE. Guides for Toxicologic Pathology. STP/ARP/AF1P; Washington, DC: 1995. Proliferative and Other Selected Lesions of the Exocrine Pancreas in Rats, GI-6.

Harada, T.; Enomoto, A.; Boorman, GA.; Maronpot, RR. Liver and Gallbladder. In: Maronpot, Robert R., editor. Pathology of the Mouse. Cache River Press; Vienna, IL: 1999. p. 119-83.

Harbord M, Novelli M, Canas B, Power D, Davis C, Godovac-Zimmermann J, Roes J, Segal AW. Ym1 is a neutrophil granule protein that crystallizes in p47phox-deficient mice. J Biol Chem. 2002; 277:5468–75. [PubMed: 11733538]

Harris MJ, Juriloff DM. An update to the list of mouse mutants with neural tube closure defects and advances toward a complete genetic perspective of neural tube closure. Birth Defects Res A Clin Mol Teratol. 2010; 88:653–69. [PubMed: 20740593]

Hoenerhoff MJ, Starost MF, Ward JM. Eosinophilic crystalline pneumonia as a major cause of death in 129S4/SvJae mice. Vet Pathol. 2006; 43:682–88. [PubMed: 16966445]

Hornick JL, Bundock EA, Fletcher CD. Hybrid schwannoma/perineurioma: Clinicopathologic analysis of 42 distinctive benign nerve sheath tumors. Am J Surg Pathol. 2009; 33:1554–561. [PubMed: 19623031]

Hosotani R, Ida J, Kogire M, Fujimoto K, Doi R, Imamura M. Expression of pancreatic duodenal hoemobox-1 in pancreatic islet neogenesis after surgical wrapping in rats. Surgery. 2004; 135:297–306. [PubMed: 14976480]

Hung SI, Chang AC, Kato I, Chang NC. Transient expression of Ym1, a heparin-binding lectin, during developmental hematopoiesis and inflammation. J Leukoc Biol. 2002; 72:72–82. [PubMed: 12101265]

Irons RD, Smith CN, Stillman WS, Shah RS, Steinhagen WH, Leiderman LJ. Macrocytic-megaloblastic anemia in male B6C3F1 mice following chronic exposure to 1,3-butadiene. Toxicol Appl Pharmacol. 1986a; 83:95–100. [PubMed: 3952753]

Irons RD, Smith CN, Stillman WS, Shah RS, Steinhagen WH, Leiderman LJ. Macrocytic-megaloblastic anemia in male NIH Swiss mice following repeated exposure to 1,3-butadiene. Toxicol Appl Pharmacol. 1986b; 85:450–55. [PubMed: 3020740]

Kemi M, Matsumoto H, Nomura Y, Takahashi R. Comparative histomorphology between Isoproterenol-induced early lesions and postmortem artifacts in the rat heart. Exp Anim. 1995; 44:240–49.

Koen H, Pugh TD, Goldfarb S. Centrilobular distribution of diethylnitrosamine-induced hepatocellular foci in the mouse. Lab Invest. 1983; 49:78–81. [PubMed: 6865333]

Langford LA, Porter S, Bunge RP. Immortalized rat Schwann cells produce tumours in vivo. J Neurocytol. 1988; 17:521–29. [PubMed: 3193129]

Lansdown AB, Grasso P. Histological observations on a Rathke's cleft abnormality in a laboratory rat. J Comp Pathol. 1971; 81:141–44. [PubMed: 5104544]

Liu Q, Cheng LI, Yi L, Zhu N, Wood A, Changpriroa CM, Ward JM, Jackson SH. p47phox deficiency induces macrophage dysfunction resulting in progressive crystalline macrophage pneumonia. Am J Pathol. 2009; 174:153–63. [PubMed: 19095958]

Louvi A, Grove EA. Cilia in the CNS: The quiet organelle claims center stage. Neuron. 2011; 69:1046–60. [PubMed: 21435552]

Luginbühl H, Detweiler DK. Cardiovascular lesions in dogs. Ann NY Acad Sci. 1965; 127:517–40. [PubMed: 5217278]

MacKenzie, WF.; Boorman, GA. Pituitary gland. In: Boorman, GA.; Eustis, SL.; Elwell, MR.; Montgomery, CA., Jr.; MacKenzie, WF., editors. Pathology of the Fischer Rat - Reference and atlas. Academic Press; San Diego, CA: 1990. p. 485-500.

Marchesi F, Monestiroli SV, Capillo M, Gobbi A, Minucci S, Pelicci PG, Scanziani E. Eosinophilic crystals as a distinctive morphologic feature of a hyaline droplet nephropathy in a mouse model of acute myelogenous leukaemia. J Vet Med A Physiol Pathol Clin Med. 2003; 50:103–107. [PubMed: 12667201]

McMartin DN, Sahota PS, Gunson DE, Han Hsu H, Spaet RH. Neoplasms and related proliferative lesions in control sprague-dawley rats from carcinogenicity studies. Historical data and diagnostic considerations. Toxicol Pathol. 1992; 20:212–25. [PubMed: 1475582]

Monis B, Valentich MA, Urrutia R, Rivolta M. Multicentric focal acinar cell hyperplasia and hepatocyte-like cell metaplasia are induced by nitrosomethylurea in rat pancreas. Int J Pancreatol. 1991; 8:119–31. [PubMed: 2033323]

Murray AB, Luz A. Acidophilic macrophage pneumonia in laboratory mice. Vet Pathol. 1990; 27:274–81. [PubMed: 2169666]

Nagatani M, Yamakawa S, Ando R, Edamoto H, Saito T, Tamura K. Highly invasive intracranial malignant schwannoma in a rat. J Toxicol Pathol. 2009; 22:139–42. [PubMed: 22271987]

Nathaniel DR. Paracrystalline arrays in atypical cristae and mitochondrial division. J Cell Sci. 1980; 42:23–32. [PubMed: 7400234]

National Toxicology Program. Technical Report 469. 1999. Accessed October, 2012. http://ntp.niehs.nih.gov/ntp/htdocs/LT_rpts/tr469.pdf

National Toxicology Program. Technical Report 570. 2011. Accessed October, 2012. http://ntp.niehs.nih.gov/ntp/htdocs/LT_rpts/TR570.pdf

Nikitin A, Lennartz K, Pozharisski KM, Rajewsky MF. Rat model of the human "Triton" tumor: direct genetic evidence for the myogenic differentiation capacity of schwannoma cells using the mutant neu gene as a cell lineage marker. Differentiation. 1991; 48:33–42. [PubMed: 1683842]

Nio J, Fujimoto W, Konno A, Kon Y, Owhashi M, Iwanaga T. Cellular expression of murine Ym1 and Ym2, chitinase family proteins, as revealed by in situ hybridization and immunohistochemistry. Histochem Cell Biol. 2004; 121:473–82. [PubMed: 15148607]

Novilla MN, Sandusky GE, Hoover DM, Ray SE, Wightman KA. A retrospective survey of endocardial proliferative lesions in rats. Vet Pathol. 1991; 28:156–65. [PubMed: 2063516]

Pollice L, Ricco R, Russo S, Maiorano E, Pagniello G, Delfino-Pesce V. Hepatocellular dysplasia: Immunohistochemical and morphometrical evaluation. Appl Pathol. 1988; 6:73–81. [PubMed: 2455530]

Reddy JK, Rao MS. Pancreatic adenocarcinoma in inbred guinea pigs induced by N-methyl-N-nitrosourea. Cancer Res. 1975; 35:2269–77. [PubMed: 1149036]

Riley, MGI.; Boonnan, GA.; McDonald, MM.; Lognecker, D.; Solleveld, HA.; Giles, HD. Guides for Toxicologic Pathology. STP/ARP/AFIP; Washington, DC: 1990. Proliferative and metaplaslic lesions of the endocrine pancreas in rats, E-1.

Sato H, Kawase S, Oku Y, Kamiya M, Ohbayashi M. Acidophilic protein crystals in lungs and bile ducts of helminth-infected mice. Nihon Juigaku Zasshi. 1988; 50:299–302. [PubMed: 3361733]

Scales SJ, de Sauvage FJ. Mechanisms of Hedgehog pathway activation in cancer and implications for therapy. Trends Pharmacol Sci. 2009; 30:303–12. [PubMed: 19443052]

Shultz LD, Coman DR, Bailey CL, Beamer WG, Sidman CL. "Viable motheaten," a new allele at the motheaten locus. I. Pathology. Am J Pathol. 1984; 116:179–92. [PubMed: 6380298]

Suski J, Lebiedzinska M, Machado NG, Oliveira PJ, Pinton P, Duszynski J, Wieckowski MR. Mitochondrial tolerance to drugs and toxic agents in ageing and disease. Curr Drug Tar. 2011; 12:827–49.

Svoboda DJ, Manning RT. Chronic alcoholism with fatty metamorphosis of the liver. Mitochondrial alterations in hepatic cells. Am J Pathol. 1964; 44:645–62. [PubMed: 5877511]

Takamoto M, Ovington KS, Behm CA, Sugane K, Young IG, Matthaei KI. Eosinophilia, parasite burden and lung damage in Toxocara canis infection in C57Bl/6 mice genetically deficient in IL-5. Immunology. 1997; 90:511–17. [PubMed: 9176103]

Teredesai A, Woehrmann T. Endocardial schwannomas in the Wistar rat. J Vet Med A Physiol Pathol Clin Med. 2005; 52:403–406. [PubMed: 16176570]

Thoolen B, Maronpot RR, Harada T, Nyska A, Rousseaux CR, Nolte T, Malarkey DE, Kaufmann W, Kuettler K, Ulrich D, Nakae D, Gregson R, Vinlove MP, Brix AE, Singh B, Belpoggi F, Ward JM. Proliferative and nonproliferative lesions of the rat and mouse hepatobiliary system. Toxicol Pathol. 2010; 38:5S–81S. [PubMed: 21191096]

Van Vleet, JF.; Ferrans, VJ.; Herman, E. Cardiovascular and Skeletal Muscle Systems. In: Haschek, WM.; Rousseaux, CG.; Wallig, MA., editors. Handbook of Toxicologic Pathology. 2nd. Academic Press; New York, NY: 2002. p. 363-456.

Veland IR, Awan A, Pederson LB, Yoder BK, Christensen ST. Primary cilia and signaling pathways in mammalian development, health and disease. Nephron Physiol. 2009; 111:39–53.

Waern I, Jia J, Pejler G, Zcharia E, Vlodavsky I, Li JP, Wernersson S. Accumulation of Ym1 and formation of intracellular crystalline bodies in alveolar macrophages lacking heparanase. Mol Immunol. 2010; 47:1467–75. [PubMed: 20226534]

Ward JM. Pulmonary pathology of the motheaten mouse. Veterinary pathology. 1978; 15:170–78. [PubMed: 664185]

Ward JM, Yoon M, Anver MR, Haines DC, Kudo G, Gonzalez FJ, Kimura S. Hyalinosis and Ym1/Ym2 gene expression in the stomach and respiratory tract of 129S4/SvJae and wild-type and CYP1A2-null B6, 129 mice. Am J Pathol. 2001; 158:323–32. [PubMed: 11141507]

Watanabe YG. The occurrence and developmental origin of epithelial cysts in the rat and mouse adenohypophysis. Arch Histol Cytol. 1991; 54:511–18. [PubMed: 1665339]

Webb DC, McKenzie AN, Foster PS. Expression of the Ym2 lectin-binding protein is dependent on interleukin (IL)-4 and IL-13 signal transduction: identification of a novel allergy-associated protein. J Biol Chem. 2001; 276:41969–76. [PubMed: 11553626]

Wickramasinghe SN. Diagnosis of megaloblastic anaemias. Blood Rev. 2006; 20:299–318. [PubMed: 16716475]

Yaeger MJ, Mullin K, Ensley SM, Ware WA, Slavin RE. Myocardial toxicity in a group of Greyhounds administered ractopamine. Vet Path. 2012; 49:569–73. [PubMed: 21997565]

Zhao J, Zhu H, Wong CH, Leung KY, Wong WS. Increased lungkine and chitinase levels in allergic airway inflammation: a proteomics approach. Proteomics. 2005; 5:2799–807. [PubMed: 15996009]

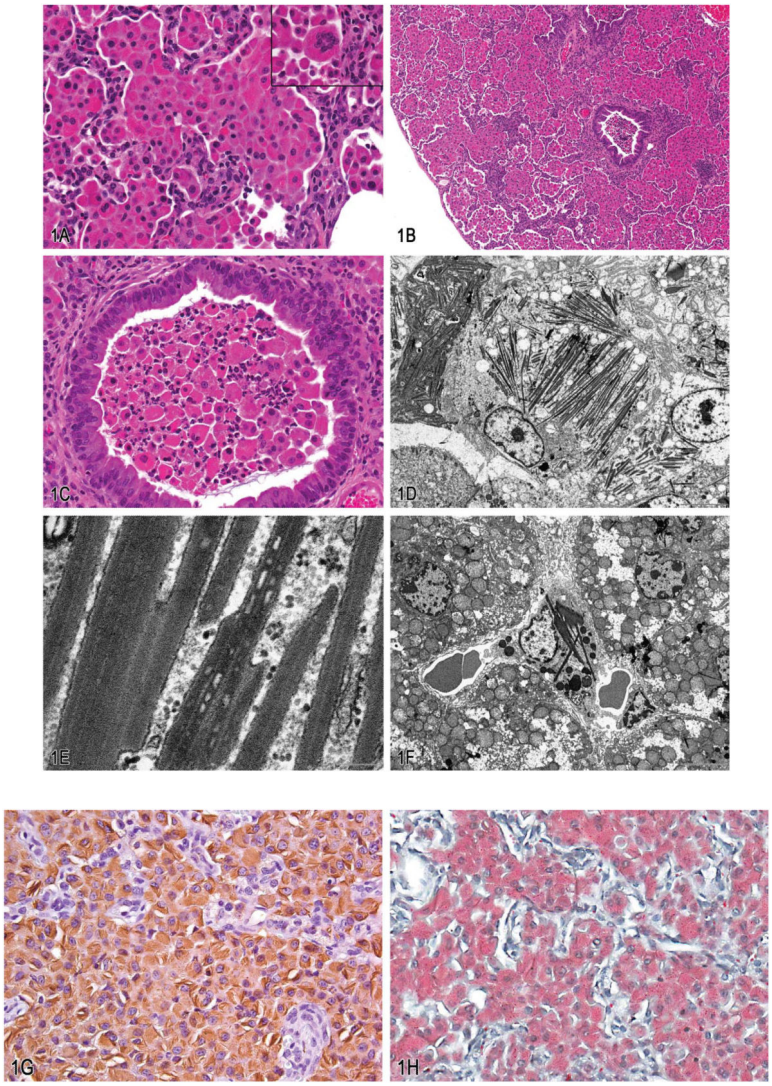

Figure 1.

Eosinophilic crystalline pneumonia in transgenic mice. A, Pulmonary alveolar spaces are markedly distended with numerous large epithelioid macrophages with brightly eosinophilic granular to amorphous cytoplasm containing fine acicular crystalline material. Occasional large binucleate and multinucleate forms were also observed (inset). Hematoxylin and eosin (H&E). B, Accompanying the marked alveolar cellular infiltrates in these mice, there was variable alveolar wall thickening with mononuclear cell infiltrates and peribronchiolar fibrosis. (H&E). C, Variable bronchiolar epithelial cell hypertrophy associated with intraluminal infiltrates consisting of aggregates of viable and degenerating macrophages and neutrophils. (H&E). D, Alveolar macrophages were markedly enlarged and distended with electron dense, needle-shaped cytoplasmic inclusions (crystalloid arrays). Transmission electron micrograph. E, Higher magnification of crystalloid arrays seen in (D). Crystalloid arrays were composed of linear stacks of granular to amorphous membrane-bound electron-dense material. Transmission electron micrograph. F, Similar electron dense crystalloid inclusions were observed in Kupffer cells lining the hepatic sinusoids. Transmission electron

micrograph. G, Labeling with antibodies against Chi3l3 protein showed moderately to markedly immunoreactive macrophages with intracytoplasmic crystalline material. H, Labeling with Luna histochemical stain showed positively stained macrophages with intracytoplasmic crystalline material.

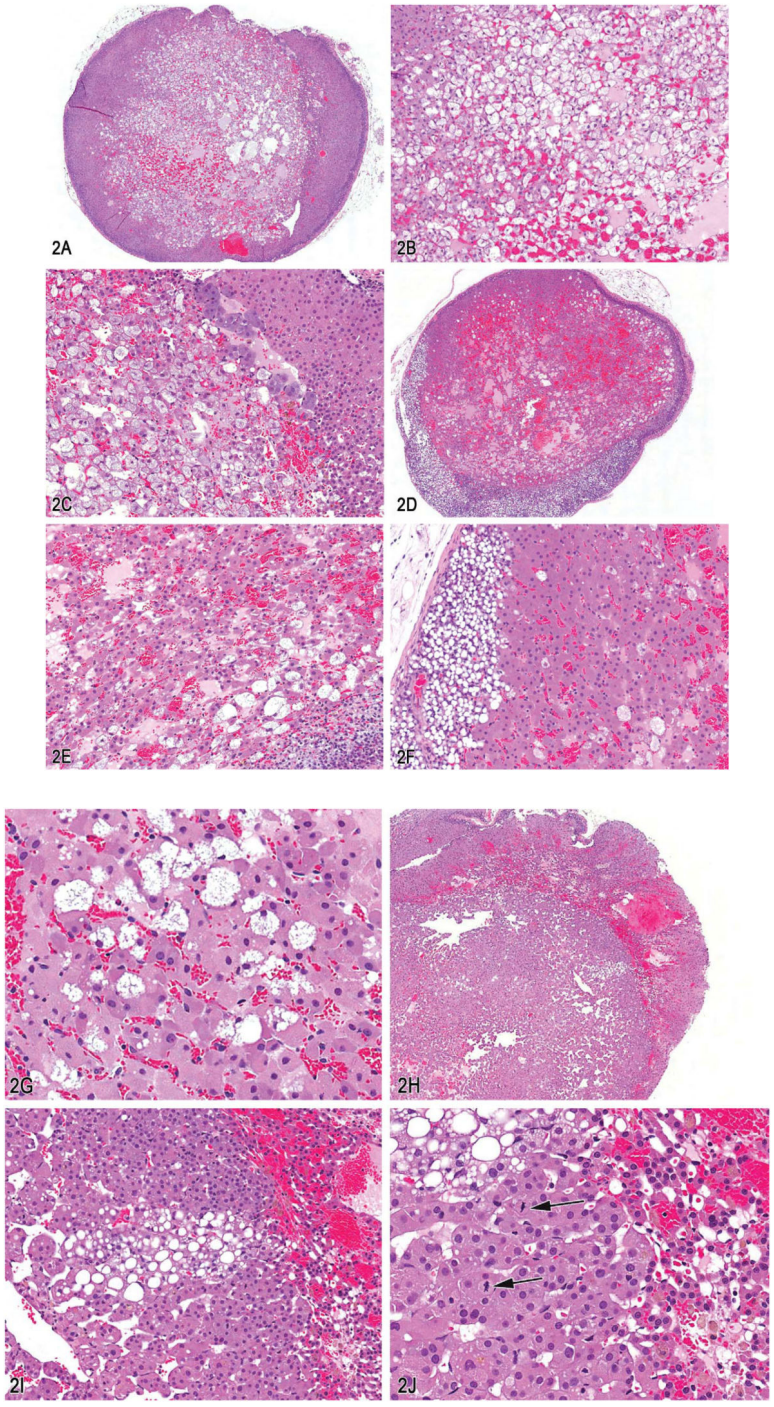

Figure 2.

A–C, Adrenal gland cortical cystic degeneration from a female Sprague-Dawley rat on a 2-yr carcinogenicity study. A, Subgross image showing a nonencapsulated, poorly demarcated lesion with cystic spaces within the cortex. B, Higher magnification of (A) showing morphology of cells, cystic spaces, and no compression of adjacent parenchyma. C, Higher magnification of (A) showing the border with the medullary region. D–G, A different presentation of adrenal gland cortical cystic degeneration from a female Sprague-Dawley rat

on a 2-yr carcinogenicity study. D, Subgross image, depicting a well-circumscribed, nonencapsulated cystic lesion within the cortex. E, Higher magnification of lesion in cortex showing cystic spaces within the lesion. F, Higher magnification of lesion at the border with the zona glomerulosa, showing atrophy and vacuolation of zona glomerulosa cells as well as hypertrophy of cells within lesion. G, Higher magnification of lesion showing cell morphology and lack of cellular atypia. H–J, Adrenal gland cortical adenoma. H, Subgross image of lesion in cortex, depicting a well demarcated lesion. I, Higher magnification of lesion in (H) showing the disorganized thick cords of cells within the lesion. J, Note the presence of mitotic figures (arrows). Hematoxylin and eosin (H&E).

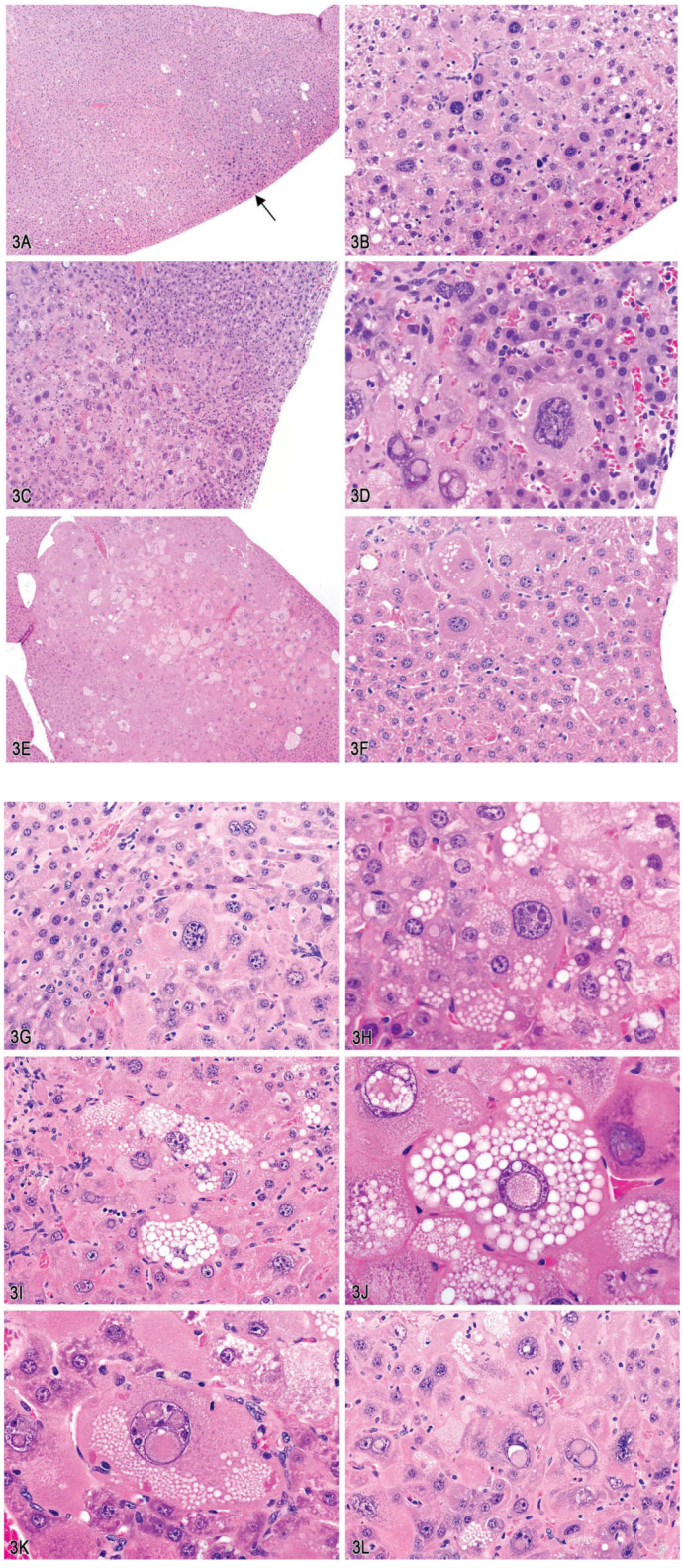

Figure 3.

Atypical foci in the livers of male and female B6C3F1 mice from 1- or 2-yr bioassays. A, Small eosinophilic atypical focus of altered hepatocytes from a mouse on a 52-week interim sacrifice study (arrow). B, Higher magnification of (A) showing cellular and nuclear atypia. C, Part of a large eosinophilic atypical focus from a mouse on a 2-yr carcinogenicity study. Note the irregular border. D, Higher magnification of (C) showing cytomegaly and karyomegaly. Note the cytoplasmic and nuclear invaginations. E, Example of a mixed cell focus with atypical cellular features from a mouse on a 2-yr study. F, Example of an atypical focus merging imperceptibly with the surrounding parenchyma. G, Example of an atypical focus causing slight compression of the surrounding parenchyma. H, Hepatocytes in atypical mixed cell foci contained multiple clear spherical vacuoles. I, Example of admixture of hepatocytes containing either solid eosinophilic cytoplasm or multiple small discrete clear vacuoles (i.e., microvesicular vacuolation). J, High magnification of intracytoplasmic vacuoles, intranuclear invaginations, and multiple nucleoli. K, Example of markedly enlarged hepatocyte with cytoplasmic vacuoles, multiple nuclear invaginations, and multiple nucleoli. Note the increase in cells adjacent to the hepatocyte (endothelium, Kupffer cells, oval cells, or biliary epithelium). L, Mid-magnification image illustrating marked cellular atypia with microvesicular vacuolation, anisocytosis, karyomegaly, multiple prominent nucleoli, and single or multiple intranuclear eosinophilic invaginations. (H&E).

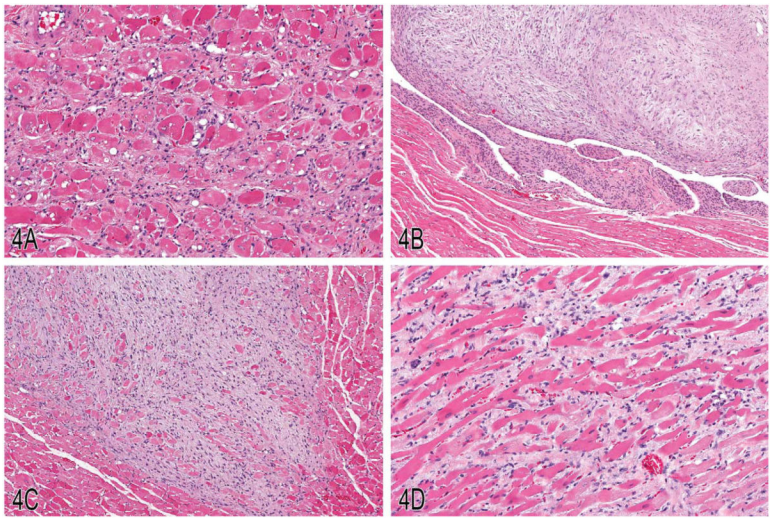

Figure 4.

Examples of “rodent progressive cardiomyopathy” (RPM), schwannoma, and cardiomyopathy in rats. A, An example of RPM characterized by a locally extensive region of cardiomyocyte necrosis and replacement by fibrosis and mononuclear infiltrates, including pigment-laden macrophages. B, A lesion diagnosed as “schwannoma” with a mildly anisocytotic and anisokaryotic subendocardial spindle cell proliferation, spanning the endocardium from the apical endocardium to the basilar endocardium. C, Example of an intramural schwannoma with interwoven bundles of neoplastic spindle cells replacing and displacing nascent cardiomyocytes. D, A lesion diagnosed as “cardiomyopathy” characterized by a regionally extensive spindle cell proliferation that dissects and displaces cardiomyocytes. (H&E).

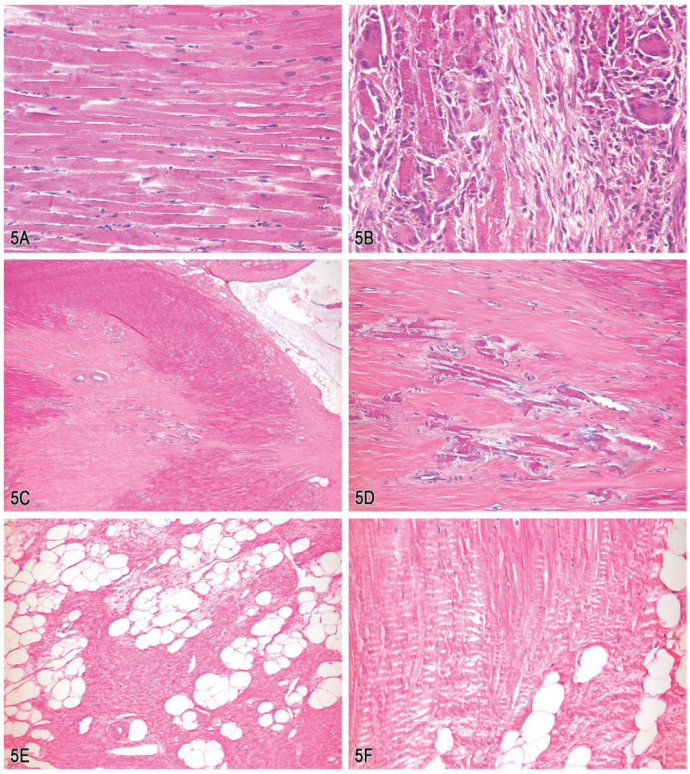

Figure 5.

Alterations in the cardiac papillary muscles from male and female Beagle dogs. A & B, Focal (acute) myocardial necrosis of the papillary muscle of a Beagle dog following a single administration of a hypotensive drug after 1 (A) and 3 days (B). C & D, Focal myocardial fibrosis with areas of mineralization in a control dog. The low magnification (C) shows the vicinity of the lesion to the insertion sites of the chordae tendinae. Figure (D) shows areas of dystrophic mineralization at a higher power. E & F, Induced degeneration of the left ventricular papillary muscles showing large areas of replacement fat (E) and the presence of mature collagen fibers in polarized light (F) after 1 yr of treatment. (H&E).

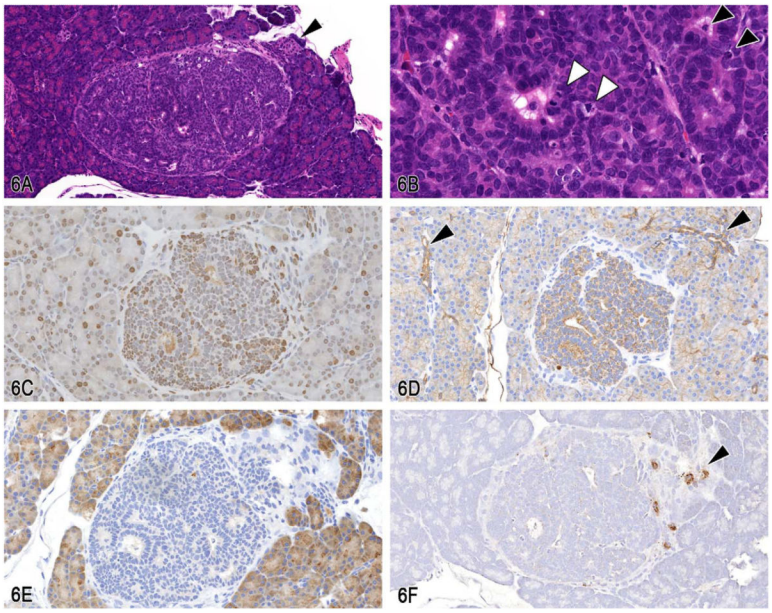

Figure 6.

Pancreatic ductal cell lesion in a 21-day-old female Lewis rat treated with *N*-methyl-*N*-nitrosourea (MNU). A, A solitary pancreatic nodule with encapsulation and slight compression of the surrounding tissue. A focus of normal islet cells are adjacent to the nodule (arrowhead; H&E). B, Cells within the nodule form ductular structures composed of cells with larger nuclei and less cytoplasm, without zymogen granules. Note the mitotic figures (white arrowheads) and apoptotic cells (black arrowheads). (H&E). C, Proliferating cell nuclear antigen (PCNA) immunohistochemistry showing many positive intralesional cells. Some surrounding acinar cells are also positive for PCNA because their cells seem to have proliferative activity at the age of 21 days. D, Pan-cytokeratin (CK) immunohistochemistry shows that cellular cytoplasm within this nodule is strongly positive for CK as well as the surrounding normal ductal cells (arrowheads). E, Immunohistochemistry using alpha-amylase shows that the cytoplasm of normal acinar cells is strongly positive for amylase; however, no signals are seen within this nodule. F, Immunohistochemistry using an insulin marker shows that no signals are detected in the cytoplasm of cells within this nodule. However, the surrounding normal islet cells are positive (arrowhead).

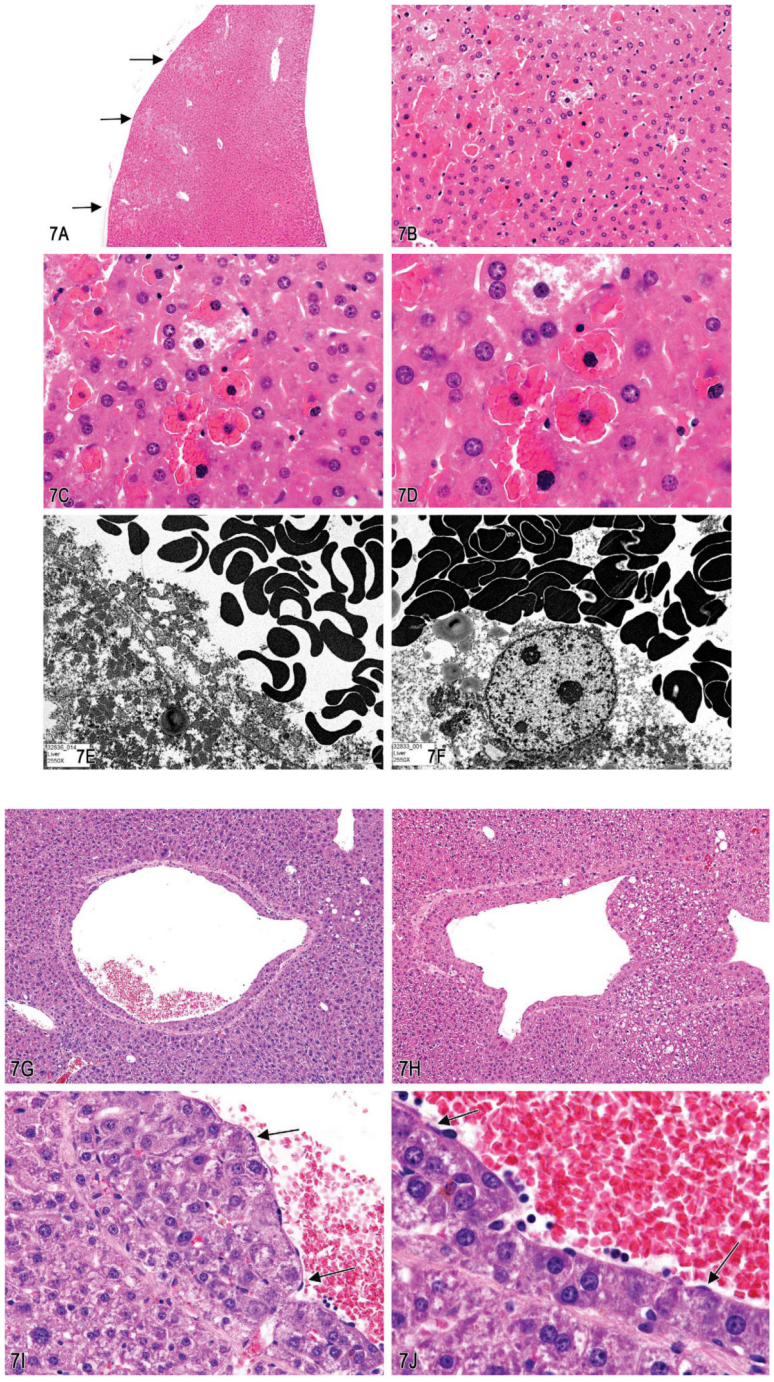

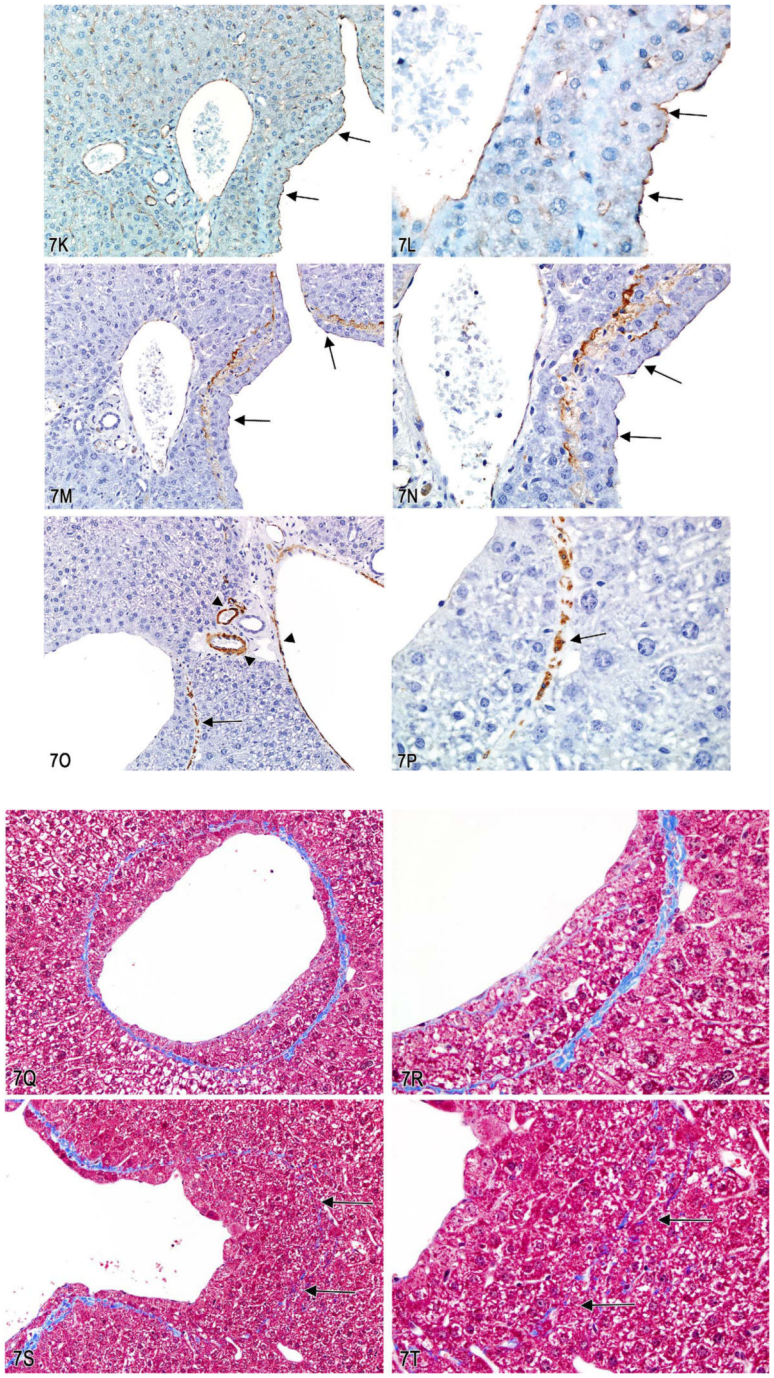

Figure 7.

A–F, Series of images characterizing the lesion of “intrahepatocytic erythrocytes.” A, Low-magnification image showing the location of several areas containing intrahepatocytic erythrocytes near the edge of the liver (arrows; H&E). B, Higher magnification of (A) illustrating intrahepatocellular erythrocytes with some adjacent hepatocytes containing a decreased cytoplasmic density. (H&E). C & D, Higher magnification images of hepatocytes containing erythrocytes within the cytoplasm. The hepatocyte nucleus is slightly condensed

and hyperchromatic and the cytoplasm is packed with erythrocytes. The remaining cytoplasm of the hepatocytes is marginated to the periphery of the cell. (H&E). E & F, Transmission electron micrographs illustrating (E) numerous erythrocytes within the hepatocellular cytoplasm and (F) that the erythrocytes are not contained within endothelial lined spaces or a lysosomal membrane. G-T, Series of images characterizing the lesion of “subendothelial hepatocytes” in the liver. G & H, Low-magnification images of the lesion illustrating hepatocytes protruding into the vessel lumen. (H&E). I & J, Higher-magnification images showing that the hepatocytes are covered with an endothelial lining (arrows). (H&E). K & L, Low- and high-magnification images of CD31 expression in endothelial cells overlying the hepatocytes lining the vessel wall (arrows). M & N, Factor VIII–related antigen expression in endothelial cells overlying the hepatocytes lining the vessel wall (arrows). O & P, Low- and high-magnification images of smooth muscle actin immunohistochemical staining of the fibromuscular portions of the hepatic vein wall (arrows). Internal positive control is an unaffected hepatic vein and portal triad vessels (arrowheads). Q–T, Trichrome stain of liver lesion with subendothelial hepatocytes. Q & R, Fibromuscular tissue of the vein wall stains positive (blue) for collagen. S & T, Migration of hepatocytes through the vein wall causes separation and displacement of the fibromuscular tissue of the vein wall in some areas (arrows).

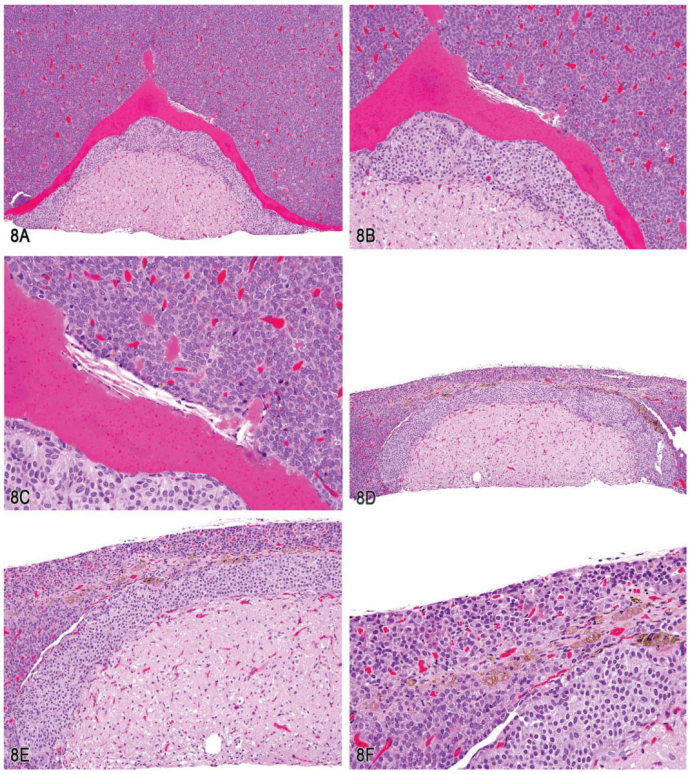

Figure 8.

Pituitary gland lesions in Rathke's cleft and pars distalis. A, Low magnification showing a dilated Rathke's cleft filled with eosinophilic proteinaceous material. B, Higher magnification of (A). C, Higher magnification of (A) showing sterol clefts and few scattered erythrocytes within the eosinophilic proteinaceous material (hemorrhage). D, Low magnification of pars distalis atrophy showing a linear pigmented area of cell loss (atrophy). E, Higher magnification of (D) showing area of cell loss and stromal collapse in the vicinity of the Rathke's cleft. F, Higher magnification of (D) revealing an area of stromal collapse containing several pigmented foamy macrophages, most likely containing hemosiderin pigment (H&E).

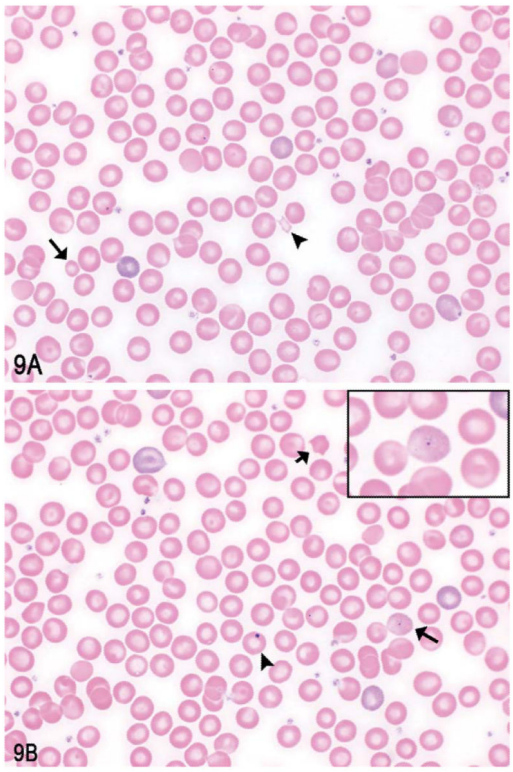

Figure 9.
Examples of erythrocyte morphology changes identified on peripheral blood smears from the B6C3F1 female mice of highdose group after 90 days of compound exposure. A, Examples of a schistocyte (arrowhead) and microcyte (arrow). B, Examples of a Howell-Jolly body (arrowhead), acanthocyte (short arrow), and basophilic stippling (long arrow, inset).

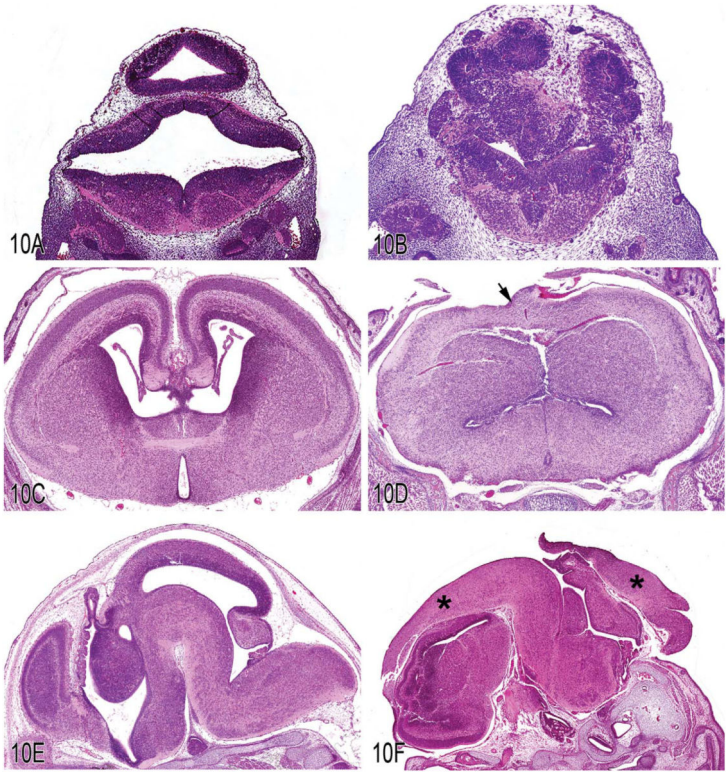

Figure 10.

Various lesions in transgenic embryos. A, Frontal section through the hindbrain of an E12.5 normal mouse embryo. B, Frontal section through the hindbrain of an E12.5 transgenic embryo. Compare with Figure 10A. Note the prominent disorganization of the neuroepithelium with numerous rosettes that are classic features of dysplasia. C, Frontal section through the forebrain of an E16.5 normal mouse embryo. D, Frontal section through the forebrain of an E16.5 transgenic mouse embryo. Compare with Figure 10C. Note that the cerebral cortex traverses the dorsal midline and there is a complete absence of normal dorsal midline differentiation (arrow). E, Parasagittal section through an E16.5 normal mouse embryo. F, Parasagittal section through an E16.5 transgenic mouse embryo. Compare with Figure 10E. Note the thick layer of neuroepithelium covering the dorsal aspect of the embryo (asterisks) and the continuity of the ventricular system with the exterior. These features are consistent with exencephaly, which is a neural tube defect localized to the cranial region (H&E).

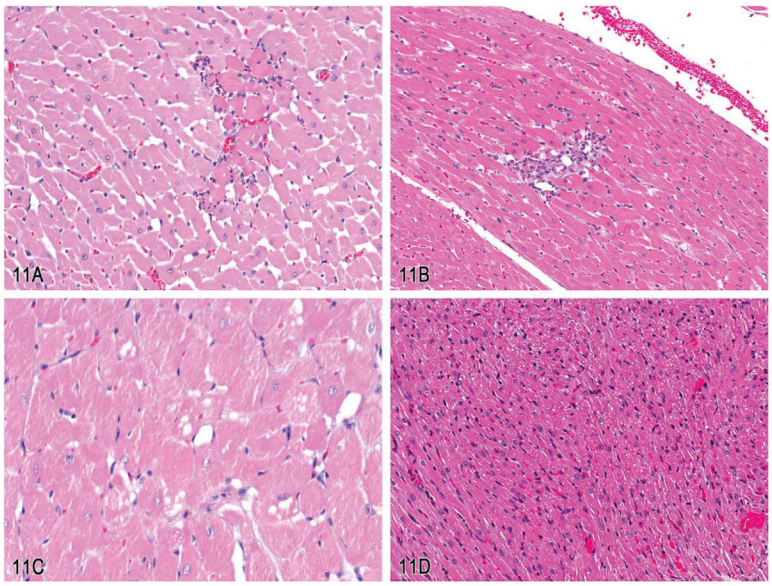

Figure 11.

Cardiovascular lesions in 10- to 12-week-old Sprague-Dawley rats. A, A well-circumscribed focus of hyaline cardiomyocyte eosinophilia with a few marginating neutrophilic inflammatory cells within the myocardium. B, A focal accumulation of mixed mononuclear inflammatory cells that have responded to and replaced a focus of cardiomyocyte necrosis. C, An area of myocardium where a number of individual cardiomyocytes are distorted by clear vacuoles that are irregular in shape and size and might be considered to expand the cellular cytoplasm. D, An area of myocardium with clear vacuoles that are present in much greater number than that compared to (C) and are more consistent in size and shape but appear to have less effect on the overall morphology of the cells (H&E).

TABLE 1

Atypical liver foci in treated mice.

	Control	Low dose	Mid dose	High dose
One-yr study				
Males	0/7[a]	2/8	4/8	6/7
Females	0/8	1/8	1/8	3/8
Two-yr study				
Males	0/50	19/50	42/49	43/51
Females	0/50	2/50	6/50	16/50

[a] Numbers denote incidence/number of animals examined.

TABLE 2

Comparison of atypical focus of cellular alteration, focus of cellular alteration, adenoma, and carcinoma.

Focus of cellular alteration, atypical
Eosinophilic or mixed cell (microvesicular) foci
Vary in size, round to oval, sometimes irregular
Hepatic plates merge imperceptibly with surrounding hepatocytes
Occasional compression
Occasional irregular borders
Cytomegaly, karyomegaly, anisocytosis, anisokaryosis
Nuclear invaginations, cytoplasmic inclusions, multiple prominent nucleoli
Focus of cellular alteration (basophilic, eosinophilic, clear, or mixed cell foci)
Vary in size, range from less than one hepatic lobule to up to several lobules in diameter
Round to oval, sometimes irregular
Hepatic plates merge imperceptibly with surrounding hepatocytes
Little or no compression
Eosinophilic foci: enlarged cells with granular pale pink cytoplasm
Clear cell foci: variable amount of cytoplasmic vacuoles (glycogen)[a]
Basophilic foci: increased cytoplasmic basophilia, cells often smaller than normal[a]
No cellular atypia[a]
Adenoma
Well-circumscribed nodules[a]
Distinct compression of adjacent parenchyma[a]
Hepatic plates at margins impinge at sharp angles to the surrounding normal liver plates[a]
Well-differentiated hepatocytes that are variable in size and tinctorial properties (eosinophilic, basophilic, clear, or admixed)
Area greater than one liver lobule
Solid or irregular plates 1–3 cells layers thick
Absence of normal lobular architecture with trapped central veins and portal tracts
May have some cellular atypia, eosinophilic cytoplasmic inclusions, mitotic figures
Carcinoma
Masses vary in size and color (eosinophilic, basophilic, vacuolated, or admixed)
Cellular atypia and mitotic figures are common
May see eosinophilic cytoplasmic inclusions
Nuclei variable in size, usually enlarged and hyperchromatic
Nucleoli distinct, larger, centrally located
Border often irregular (distinct invasion and compression)[a]
May have necrosis and hemorrhage[a]
Abnormal growth pattern: trabecular, glandular, and/or solid[a]
Trabecular pattern 3 or more cell layers thick[a]
May see pulmonary metastases[a]

[a] Features that are distinctly different from atypical foci.

TABLE 3

Criteria for pancreatic duct proliferative lesions.

Diagnosis	Proliferative activity	Compression	Encapsulation	Invasion	Cellular atypia
Hyperplasia	+/−	−	−	−	−
Adenoma	+	+	+	−	−
Adenocarcinoma	+	+	−	+	+
This case	+	+	+	−	−

TABLE 4

Incidences of intrahepatocytic erythrocytes: Short-term NTP studies.

Chemical	Control	Low	Low-mid	Mid	Mid-high	High
Nelfinavir immunotoxicity 28-day study; female mice	0/8	3/8	N/A	4/8	N/A	4/8
Propargyl alcohol 14-day study; male mice	0/5	NE	0/5	3/5	5/5	5/5
Propargyl alcohol 14-day study; female mice	0/5	NE	0/5	5/5	N/A	N/A
Propargyl alcohol 14-day study; male rats	0/5	NE	0/5	0/5	5/5	5/5
Propargyl alcohol 14-day study; female rats	0/5	NE	0/5	0/5	5/5	5/5

Note: NE = not examined; N/A = not applicable; NTP = National Toxicology Program.

TABLE 5

Incidences of intrahepatocytic erythrocytes: 2-yr mouse NTP studies.

Chemical	Control	Low	Mid	High
Resorcinol; males	0/50	NE	0/50	3/50
1-Chloro-2-propanol; males	0/50	1/50	0/50	0/50
Ethylene Glycol; males	0/50	0/50	0/51	2/50
Tricresyl phosphate; males	0/52	0/49	0/49	1/50
Alpha methylstyrene; males	1/42	0/41	0/45	0/39
Cumene; females	0/50	0/50	0/50	1/50
Decalin; males	0/50	0/50	0/50	9/50
Anthraquinone; males	1/50	9/50	13/50	6/49
Methyl isobutyl ketone; males	0/43	0/44	0/39	1/45
Ginko biloba; males	0/50	4/50	11/50	7/50
Ginko biloba; females	0/50	3/50	7/50	16/50

Note: NE = not examined; NTP = National Toxicology Program.

TABLE 6

Hematology data from B6C3F1 female mice after 90 days of compound exposure.[a]

Parameter	Control	1,000 mg/kg
RBC count, × 10^6/μl	10.49	8.36*
Hemoglobin, g/dl	15.5	14.2*
Hematocrit, %	47.4	44*
MCV, fL/cell	45.2	52.6*
MCH, pg/cell	14.8	17*
MCHC, g/dl	32.7	32.4
Reticulocytes, × 10^3/μ1	266.2	249.7

Note: MCV = mean cell volume; MCH = mean cell hemoglobin; MCHC = mean cell hemoglobin concentration.

*Significantly ($p \leq .01$) different from control group.

[a]Data presented as mean values.